AD-A032 553 CALSPAN CORP BUFFALO N Y F/G 20/4
RELAXATION SOLUTIONS FOR THREE-DIMENSIONAL TRANSONIC FLOW THROU--ETC(U)
AUG 76 W J RAE F44620-74-C-0059
UNCLASSIFIED CALSPAN-AB-5487-A-2 AFOSR-TR-76-1081 NL

1 OF 1
ADA032553

END

DATE
FILMED
1 -77

AFOSR - TR - 76 - 1081

Calspan

Technical Report

Approved for public release;
distribution unlimited.

Calspan Corporation
Buffalo, New York 14221

Calspan

RELAXATION SOLUTIONS FOR THREE-DIMENSIONAL TRANSONIC FLOW THROUGH A COMPRESSOR BLADE ROW, IN THE NONLINEAR SMALL-DISTURBANCE APPROXIMATION

William J. Rae

Calspan Report No. AB-5487-A-2

AUGUST 1976

Prepared For:

AIR FORCE OFFICE OF SCIENTIFIC RESEARCH
BOLLING AIR FORCE BASE, D.C. 20332

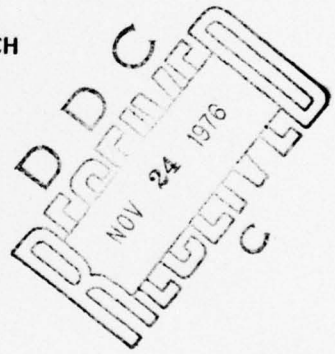

CONTRACT NO. F44620-74-C-0059
INTERIM SCIENTIFIC REPORT

Calspan Corporation
Buffalo, New York 14221

UNCLASSIFIED

SECURITY CLASSIFICATION OF THIS PAGE *(When Data Entered)*

REPORT DOCUMENTATION PAGE

READ INSTRUCTIONS BEFORE COMPLETING FORM

1. REPORT NUMBER (19) AFOSR-TR-76-1081	2. GOVT ACCESSION NO.
3. RECIPIENT'S CATALOG NUMBER	
4. TITLE (and Subtitle) (6) RELAXATION SOLUTIONS FOR THREE-DIMENSIONAL TRANSONIC FLOW THROUGH A COMPRESSOR BLADE ROW, IN THE NONLINEAR SMALL-DISTURBANCE APPROXIMATION.	5. TYPE OF REPORT & PERIOD COVERED (9) INTERIM scientific rept.
	6. PERFORMING ORG. REPORT NUMBER AB-5487-A-2
7. AUTHOR(s) (10) WILLIAM J. RAE	8. CONTRACT OR GRANT NUMBER(s) (15) F44620-74-C-0059
9. PERFORMING ORGANIZATION NAME AND ADDRESS CALSPAN CORPORATION P O BOX 235 BUFFALO, NEW YORK 14221	10. PROGRAM ELEMENT, PROJECT, TASK AREA & WORK UNIT NUMBERS (16) 681307 (17) 9781-01 61102F
11. CONTROLLING OFFICE NAME AND ADDRESS AIR FORCE OFFICE OF SCIENTIFIC RESEARCH/NA BUILDING 410 BOLLING AIR FORCE BASE, D C 20332	12. REPORT DATE (11) Aug 76
	13. NUMBER OF PAGES 43 (12) 51 p.
14. MONITORING AGENCY NAME & ADDRESS *(if different from Controlling Office)*	15. SECURITY CLASS. *(of this report)* UNCLASSIFIED
	15a. DECLASSIFICATION/DOWNGRADING SCHEDULE

16. DISTRIBUTION STATEMENT *(of this Report)*

Approved for public release; distribution unlimited.

(14) CALSPAN-AB-5487-A-2

17. DISTRIBUTION STATEMENT *(of the abstract entered in Block 20, if different from Report)*

18. SUPPLEMENTARY NOTES

19. KEY WORDS *(Continue on reverse side if necessary and identify by block number)*

TURBOMACHINERY
COMPRESSORS
TRANSONIC FLOW
FINITE-DIFFERENCE SOLUTIONS

20. ABSTRACT *(Continue on reverse side if necessary and identify by block number)*

A relaxation method for calculating the three-dimensional transonic flow through a compressor blade row is discribed. The flow is taken to be steady in blade-fixed coordinates, and is treated in the nonlinear small-disturbance approximation. Details of the finite-difference formulation and the solution procedure are given. The resulting computer code is capable of operating in either of two modes: in the first, the user specifies the complete blade shape and the operating conditions, and the program finds the complete flow field, including the loading distribution on the blades. In the second, the user specifies the loading distribution over → next page

DD FORM 1 JAN 73 1473 EDITION OF 1 NOV 65 IS OBSOLETE

UNCLASSIFIED

SECURITY CLASSIFICATION OF THIS PAGE *(When Data Entered)*

407 727

the blade surface, and the thickness distribution of the blades. The program then finds the three-dimensional flow field, including the shape of the camber surface about which the prescribed thickness must be symmetrically distributed, in order to produce the prescribed loading. Results of demonstration calculations illustrating each of these modes are included.

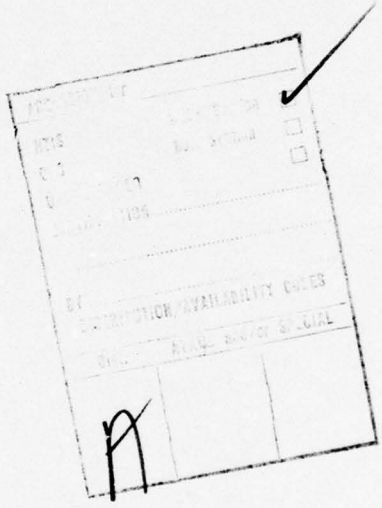

ABSTRACT

A relaxation method for calculating the three-dimensional transonic flow through a compressor blade row is described. The flow is taken to be steady in blade-fixed coordinates, and is treated in the nonlinear small-disturbance approximation. Details of the finite-difference formulation and the solution procedure are given. The resulting computer code is capable of operating in either of two modes: in the first, the user specifies the complete blade shape and the operating conditions, and the program finds the complete flow field, including the loading distribution on the blades. In the second, the user specifies the loading distribution over the blade surface, and the thickness distribution of the blades. The program then finds the three-dimensional flow field, including the shape of the camber surface about which the prescribed thickness must be symmetrically distributed, in order to produce the prescribed loading.

Results of demonstration calculations illustrating each of these modes are included.

LIST OF SYMBOLS

a_∞	speed of sound far upstream
B	number of blades
C_a	axial projection of the chord
$h(s)$	camber line shape
K, L, N	indices numbering the grid points in the z , ζ , ρ directions
L_T	$2\pi r_T / B$
M_∞	u_∞ / a_∞
$\eta(s)$	blade shape
p	pressure
r, θ, x	cylindrical coordinates
s, n	streamwise and normal coordinates in a surface at constant radius
$t(s)$	blade thickness shape
u, v, w	perturbation velocity components in the z , ρ , θ directions
u_n, u_s	perturbation velocity components in the streamwise and normal directions, in a constant-radius surface
u_∞	axial flow speed far upstream
W_z, W_r, W_θ	components of the relative velocity seen by a blade-fixed observer
W_o	$(u_\infty^2 + \omega^2 r^2)^{1/2}$
z	$\omega x / u_\infty$
Γ	circulation
γ	specific-heat ratio
$\Delta\phi(\rho)$	jump in potential across the trailing vortex sheet
ζ	$\theta - z$
ρ	$\omega r / u_\infty$

ρ_∞ density far upstream

φ, ϕ velocity potential

ω angular velocity of the approach flow, seen by a blade-fixed observer. Also used to denote a relaxation factor.

$()_{H,T}$ denote evaluation at the hub, tip

$()_{u,L}$ denotes evaluation on the upper, lower surface of a blade

TABLE OF CONTENTS

INTRODUCTION

The flow in transonic turbomachinery is one in which most of the difficult complications in fluid mechanics occur simultaneously. The flow is in general transonic, three-dimensional, and unsteady; the effects of viscosity are felt in shock-wave and boundary-layer phenomena which are, themselves, three-dimensional and unsteady. And the three-dimensionality may appear in the form of velocity distortions and entropy gradients in the inlet flow itself.

Despite these complications, axial-flow machines run with very attractive levels of performance. However, increasing demands for improved performance, with decreased weight, noise, and fuel consumption,[1,2,3] continue to place great emphasis on the importance of understanding these complex flow problems.

In seeking approaches that may assist this understanding, it is natural to turn to methods which have already proven their value in studies of the external flow over wings and bodies. These methods can, in some cases, be adapted to the special circumstances of turbomachinery flows; when this can be done, a wide variety of analytical tools and a great wealth of understanding is brought to bear on the problem.

The present study is one such attempt. During the past decade, the field of external transonic flows has undergone a revolution, centered on the use of numerical methods of flowfield prediction. One of the key contributions that set these advances in motion was the development, by Krupp, Murman, and Cole[4-7] of relaxation methods that were capable of handling the mixed elliptic/hyperbolic character of transonic flow. These early works, all done in the nonlinear small-disturbance approximation, clarified many features of transonic flow, such as shock-wave and sonic-line locations, and the relations between surface geometry and surface loading. They also served as the necessary external-flow adjunct for boundary-layer studies, and for predictions of shock-wave/boundary-layer interaction phenomena. The experience gained in the

small-disturbance approximation soon led to advances into the more fully nonlinear aspects of the problem, and into such further complications as three-dimensionality.

The basic purpose of the present work is to apply that same first step to turbomachinery flows, i.e., to develop a three-dimensional relaxation method for transonic small-disturbance flow through a turbomachine blade row. The simplicity offered by the small-disturbance approximation facilitates the adaptation of external-flow computational methods, and indicates fruitful directions for higher-order extensions. At the same time, the restrictions implicit in the small-disturbance formulation limit the range of validity of its results to low turning angles and total pressure ratios near one. The precise limits of this range will have to be determined, by comparison with experiment and with the predictions of more complete models. In the meantime, results found in the small-disturbance approximation can be expected to produce useful information about three-dimensional shock patterns, boundary-layer behavior, and the interaction between adjacent supersonic and subsonic zones.

This paper begins with a summary and description of how the small-disturbance formulation, given in Part I (Ref. 8), has been cast into finite-difference form. This section also contains comments on some of the essential programming steps that went into the computer code developed.

Section II contains results from two demonstration calculations that were made for the purpose of illustrating the computer-program capability. These results include examples of supercritical flow in the blade passages, and serve as a basis for estimating the computing time required to do a given calculation.

The concluding remarks indicate two avenues of research which are opened up by the successful demonstration of this technique. One of them lies in the general direction of further extensions of the method; this area includes such topics as the incorporation of the full nonlinearity, and an accounting for some of the shock-wave and boundary-layer phenomena that play

such an important role in turbomachinery performance. The second direction consists of applications of the present capability. The availability of this method makes it possible to conduct, at very modest cost, parametric design studies of the blade shapes required to produce a given loading, and of the off-design performance of these blade rows, all in the presence of three-dimensionality and the occurrence of mixed subsonic/supersonic flow. While these calculations are limited to the range of validity of the small-disturbance equations, they nevertheless offer an immediate method for learning in detail about the intricacies of this complicated flow field. There is much to be learned from such an application, and the opportunity need not be deferred until after the more advanced approximations come into existence.

I. FINITE-DIFFERENCE FORMULATION

The coordinate system and rotor geometry used are shown in Figure 1, where the dimensionless variables are defined as

$$\bar{z} = \frac{\omega x}{U_\infty} \quad , \quad \rho = \frac{\omega r}{U_\infty} \quad , \quad \zeta = \theta - \bar{z} \quad ; \quad \phi = \frac{\omega \varphi}{U_\infty} \tag{1}$$

The velocity components seen by a blade-fixed observer are

$$W_x = U_\infty + u \quad , \quad W_r = v \quad , \quad W_\theta = \omega r + w \tag{2}$$

These dimensional perturbation velocities are related to the velocity potential by

$$\bar{u} = \frac{u}{U_\infty} = \left.\frac{\partial \phi}{\partial \bar{z}}\right)_{\rho,\theta} = \left.\frac{\partial \phi}{\partial \bar{z}}\right)_{\rho,\zeta} - \left.\frac{\partial \phi}{\partial \zeta}\right)_{\bar{z},\rho} ;$$

$$\bar{v} = \frac{v}{U_\infty} = \left.\frac{\partial \phi}{\partial \rho}\right)_{\bar{z},\theta} = \left.\frac{\partial \phi}{\partial \rho}\right)_{\bar{z},\zeta} \tag{3}$$

$$\bar{w} = \frac{w}{U_\infty} = \left.\frac{1}{\rho}\frac{\partial \phi}{\partial \theta}\right)_{\bar{z},\rho} = \left.\frac{1}{\rho}\frac{\partial \phi}{\partial \zeta}\right)_{\bar{z},\rho}$$

The velocity potential satisfies the equation

$$\left\{1 - M_\infty^2 (1+\rho^2) - (\gamma+1) M_\infty^2 \phi_{\bar{z}}\right\} \phi_{\bar{z}\bar{z}} + \rho^2 \phi_{\bar{z}\bar{z}} - 2(1+\rho^2)\phi_{\zeta\bar{z}} + \frac{(1+\rho^2)^2}{\rho^2}\phi_{\zeta\zeta} + (1+\rho^2)\left(\phi_{\rho\rho} + \frac{1}{\rho}\phi_\rho\right) = 0 \tag{4}$$

Subscripts denote derivatives in the $\bar{z}$, ρ , ζ coordinate system; thus the symbol $\phi_{\bar{z}}$ stands for $\left.\frac{\partial \phi}{\partial \bar{z}}\right)_{\rho,\zeta}$. There are B blades in the row, and they are taken to lie in the helical surfaces defined by U_∞ and ωr . The axial projection of their chord is a constant, C_a . Thus, they are located at

$$0 \le \bar{z} \le \frac{\omega C_a}{U_\infty} \quad ; \quad \rho_H \le \rho \le \rho_T \quad ; \quad \zeta = \frac{2j\pi}{B} \quad , \quad j = 0, 1, 2, \ldots, B-1 \tag{5}$$

For purposes of numerical calculation, attention is restricted to the region between two blades ($0 \leq \zeta \leq \frac{2\pi}{B}$), and the solution is made periodic in successive intervals of $2\pi/B$. In the small-disturbance approximation, the blade-surface boundary conditions are enforced in the surfaces $\zeta = 0$ and $\zeta = 2\pi/B$.

The region in which the solution is to be found is now divided into a grid, as shown in Figure 2, where the indices L , K , and N are used to number the points in the ζ , z , and ρ directions, respectively. Values of the potential at each of these grid points are denoted by

$$\phi(z, \rho, \zeta) = \phi(L, K, N) = {}^{N}\phi^{L}_{K}$$

The use of this grid makes it very easy to enforce the periodicity conditions; for example, when solving for the flow in the blade-to-blade plane at constant ρ , the periodicity condition upstream of the blade row (see Equation 49 of Reference 8) requires that $\phi(1, K, N) = \phi(LMX, K, N)$, where $L = 1$ and $L = LMX$ are the indices corresponding to $\zeta = 0$ and $\zeta = 2\pi/B$. However, the skew coordinate system leads to a misalignment between the fore Mach cone through a given point and the grid points in the ζ-direction. It is known from external-flow studies[9-11] that a misalignment of this sort will lead to an unstable iteration process, even though derivatives in the z -direction at constant ζ are taken in the upwind direction.

The remedy for this problem is to use the rotated-difference scheme introduced by Jameson.[9] His method was developed for the case where the flow velocity displays large deflections from one of the coordinate directions (see Figure 3, which shows a rectangular coordinate system for convenience). Jameson's basic contribution was to replace the partial differential equation in x and y by one in the streamline, normal coordinates s , n . The potential equation can then be expressed locally in the form

$$\left(1 - \frac{q^2}{a^2}\right)\phi_{ss} + \phi_{nn} + \cdots = 0$$

where the three dots stand for lower-order derivatives, and where the second

derivatives are related to their local counterparts in the rectangular system by

$$\phi_{ss} = \frac{1}{q^2}\left(q_x^2\,\phi_{xx} + 2\,q_x q_y\,\phi_{xy} + q_y^2\,\phi_{yy}\right)$$

$$\phi_{nn} = \frac{1}{q^2}\left(q_y^2\,\phi_{xx} - 2\,q_x q_y\,\phi_{xy} + q_x^2\,\phi_{yy}\right)$$

where q is the magnitude of the local velocity vector and q_x and q_y are its x and y components. After expressing the potential equation this way, contributions to the ϕ_{ss} term are then represented by upwind differences, while terms contributing to ϕ_{nn} are evaluated by central differences.

For the present case, the misalignment between the fore Mach cone and the z = constant grid points is not caused by large flow deflections, but by the skew nature of the grid. The same general principles can be applied, however; the contributions to ϕ_{ss} and ϕ_{nn} can be identified by writing (in dimensional variables):

$$\varphi_{ss} = \frac{1}{W_o^2}\left\{u_\infty^2\,\varphi_{xx} + 2\,u_\infty\,\omega\,\varphi_{x\theta} + \omega^2\varphi_{\theta\theta}\right\}$$

$$\varphi_{nn} = \frac{1}{W_o^2}\left\{(\omega r)^2\varphi_{xx} - 2\,\omega\,u_\infty\,\varphi_{x\theta} + \frac{u_\infty^2}{r^2}\,\varphi_{\theta\theta}\right\}$$

where $W_o^2 = u_\infty^2 + (\omega r)^2$. Note that the small-disturbance approximation has already been used here, by neglecting the contribution of the perturbation velocities to these formulas. If these are now re-written in dimensionless form, and transformed to the $\bar{z}$, ρ , ξ coordinates, it is found that

$$\varphi_{ss} = \frac{\omega\,u_\infty^2}{W_o^2}\,\phi_{\bar{z}\bar{z}} \quad ;$$

$$\varphi_{nn} = \frac{\omega\,u_\infty^2}{W_o^2}\left\{\rho^2\phi_{\bar{z}\bar{z}} - 2(1+\rho^2)\,\phi_{\xi\bar{z}} + \left(\rho^2 + 2 + \frac{1}{\rho^2}\right)\phi_{\xi\xi}\right\} \qquad (6)$$

Thus, it is clear that the potential equation, as displayed in Equation (4), is already in a form suitable for the application of Jameson's technique: the first term in Equation (4) is to be evaluated by upwind or central differences, depending on whether the local Mach number is supersonic or subsonic, while all the remaining terms are to be evaluated by central difference formulas.

In addition to these considerations, it is essential that the difference scheme be fully conservative,[12,13] in order to avoid the spurious introduction of additional mass flow. Thus, the potential equation is re-written in the divergence form:

$$\frac{\partial}{\partial z}\left\{\left[1-M_\infty^2(1+\rho^2)\right]\phi_z-\frac{\gamma+1}{2}M_\infty^2\phi_z^2\right\}-\frac{\partial}{\partial z}\left\{\rho(1+\rho^2)\left[\frac{1}{\rho}\phi_\zeta-\frac{\rho}{1+\rho^2}\phi_z\right]\right\}$$

$$+\frac{\partial}{\partial\zeta}\left\{\frac{(1+\rho^2)^2}{\rho}\left[\frac{1}{\rho}\phi_\zeta-\frac{\rho}{1+\rho^2}\phi_z\right]\right\}+\frac{1+\rho^2}{\rho}\frac{\partial}{\partial\rho}(\rho\phi_\rho)=0 \tag{7}$$

The grid used throughout the present work has uniformly spaced points in the radial and blade-to-blade directions, and a nonuniform spacing in the z-direction. The z-coordinate is taken to be related to a transformed coordinate τ, such that

$$\frac{\partial}{\partial z}=f\frac{\partial}{\partial\tau}\quad;\quad f\equiv\frac{d\tau}{dz} \tag{8}$$

A constant grid spacing $\Delta\tau$ is then used, giving rise to a nonuniform spacing in z. The computer program as written contains a specific transformation, described below, in one of the subroutines. Other transformations can be used by making appropriate changes in this subroutine, whose purpose is to return the function f.

Using the variable τ, the potential equation becomes:

$$\frac{\partial}{\partial\tau}\left\{f\left[1-M_\infty^2(1+\rho^2)-\frac{\gamma+1}{2}M_\infty^2 f\frac{\partial\phi}{\partial\tau}\right]\frac{\partial\phi}{\partial\tau}\right\}$$

$$-\rho(1+\rho^2)\frac{\partial}{\partial\tau}\left\{\frac{1}{\rho}\phi_\zeta-\frac{\rho}{1+\rho^2}\frac{\partial}{\partial\tau}\left(f\frac{\partial\phi}{\partial\tau}\right)\right\}+\frac{(1+\rho^2)^2}{\rho f}\frac{\partial}{\partial\zeta}\left\{\frac{1}{\rho}\phi_\zeta-\frac{\rho f}{1+\rho^2}\frac{\partial\phi}{\partial\tau}\right\}$$

$$+\frac{(1+\rho^2)}{\rho f}\frac{\partial}{\partial\rho}(\rho\phi_\rho)=0 \tag{9}$$

The first term in this equation is to be evaluated by type-dependent differences. In order to retain mass conservation, it is necessary to use the shock-point operator at points where the flow changes from supersonic to subsonic values.[12] Jameson[14] has pointed out a simple way of doing so, using a switching function

μ which is defined to be zero in subsonic flow and 1 in supersonic flow. Using these concepts, plus the formulas suggested by South and Jameson,[11] the following finite-difference form of the potential equation results:

$$
\begin{aligned}
&\left\{\beta_o^2 - b f_K \frac{{}^N\phi^L_{K+1} - {}^N\phi^L_{K-1}}{2\Delta\tau}\right\}\left\{(1-\mu^L_K)\left\langle f_{K+1/2}\,{}^N\phi^L_{K+1} - 2f_K\left[\frac{{}^N\phi^{+L}_K}{\omega_e} + \left(1-\frac{1}{\omega_e}\right){}^N\phi^L_K\right] + f_{K-1/2}\,{}^N\phi^{+L}_{K-1}\right\rangle\right.\\
&\left. + \mu^L_{K-1}\left\langle f_{K-1/2}\left({}^N\phi^{+L}_K - {}^N\phi^L_K - {}^N\phi^{+L}_{K-1}\right) - f_{K-3/2}\left({}^N\phi^{+L}_{K-1} - {}^N\phi^L_{K-2}\right)\right\rangle\right\}\\
&+ \rho^2(1-\mu^L_K)\left\{f_{K+1/2}\,{}^N\phi^L_{K+1} - 2f_K\left[\frac{{}^N\phi^{+L}_K}{\omega_e} + \left(1-\frac{1}{\omega_e}\right){}^N\phi^L_K\right] + f_{K-1/2}\,{}^N\phi^{+L}_{K-1}\right\}\\
&+ \rho^2\mu^L_K\left\{f_{K+1/2}\left({}^N\phi^L_{K+1} - {}^N\phi^L_K\right) - f_{K-1/2}\left({}^N\phi^{+L}_K - {}^N\phi^{+L}_{K-1}\right)\right\}\\
&- \frac{(1+\rho^2)\Delta\tau}{2\Delta\zeta}\left\{{}^N\phi^{L+1}_{K+1} - {}^N\phi^{L-1}_{K+1} - {}^N\phi^{+L+1}_{K-1} + {}^N\phi^{+L-1}_{K-1}\right\}\\
&+ \frac{(1+\rho^2)^2}{\rho^2 f_K}\left(\frac{\Delta\tau}{\Delta\zeta}\right)^2\left\{{}^N\phi^{+L+1}_K - 2\,{}^N\phi^{+L}_K + {}^N\phi^{+L-1}_K\right\}\\
&+ \frac{(1+\rho^2)}{f_K}\left(\frac{\Delta\tau}{\Delta\rho}\right)^2\left\{\left(1+\frac{\Delta\rho}{2\rho}\right){}^{N+1}\phi^L_K + \left(1-\frac{\Delta\rho}{2\rho}\right){}^{N-1}\phi^L_K - 2\,{}^N\phi^L_K\right\} = 0
\end{aligned}
\tag{10}
$$

where $\beta_o^2 \equiv 1 - M_\infty^2(1+\rho^2)$, $b \equiv (\gamma+1)M_\infty^2$, $\mu^L_K = \begin{matrix}1\\0\end{matrix}$, $M \gtrless 1$. A plus sign over a term indicates that its value is to be updated on the current iteration, or set equal to its value on the current iteration, if it has already been updated, as in the case of the term ${}^N\phi^{+L}_{K-1}$. The quantity ω_e is the relaxation factor used at elliptic points.

Line Relaxation

The sequence of iterations to be followed in the relaxation solution is as follows: starting at a given radius, all the points on the line z = constant will be solved for by line relaxation. This line will be swept downstream, and the sweep repeated a number of times before moving to the next radius. Thus, it is convenient to arrange the potential equation in a tridiagonal form

$$A_K^L \, {}^N\phi_K^{+L+1} + B_K^L \, {}^N\phi_K^{+L} + C_K^L \, {}^N\phi_K^{+L-1} = D_K^L \,, \qquad L = 2, 3, \cdots, LMX - 1 \tag{11}$$

where LMX is the index corresponding to $\zeta = 2\pi/\beta$. The coefficients A_K^L , B_K^L , C_K^L , and D_K^L are all known, in terms of the independent variables, and values of ϕ at neighboring points in the grid found on the previous z - sweep (or, in the case of some terms at $K-1$, found on the current z - sweep). The explicit forms of these coefficients depend on whether the flow is locally hyperbolic or elliptic. This is decided by the sign of the centered-difference form of the coefficient of ϕ_{zz} :

$$V \equiv 1 - M_\infty^2 (1 + \rho^2) - (\gamma + 1) M_\infty^2 \, f_K \, \frac{{}^N\phi_{K+1}^L - {}^N\phi_{K-1}^L}{2\Delta\tau} \tag{12}$$

where ϕ_z is evaluated from the values that were found on the previous z - sweep. If V is positive, the point is elliptic, and centered differences are used throughout; if V is negative, the point is hyperbolic, and upwind differences are used for ϕ_{zz} .

The tridiagonal solution is found in the usual way (see Reference 15, for example). Let

$${}^N\phi_K^{+L} = E(L) \, {}^N\phi_K^{+L+1} + F(L) \tag{13}$$

Then the quantities E and F obey the recursion relations:

$$E(L) = -A_K^L \Big/ \left[B_K^L + C_K^L \, E(L-1)\right] \tag{14}$$

$$F(L) = \left[D_K^L - C_K^L \, F(L-1)\right] \Big/ \left[B_K^L + C_K^L \, E(L-1)\right] \tag{15}$$

The boundary or periodicity conditions at $L = 1$ are used to set $E(1)$ and $F(1)$. Then the recursion formulas [Equations (14) - (15)] give $E(L)$ and $F(L)$ for $L = 2, 3, \ldots, LMX-1$. Boundary or periodicity conditions at $L = LMX$ are then used to set ϕ at LMX, and then Equation (13) is used to work back down to $L = 2$. After these (tentative) values of ϕ have been found, (and stored in an array $S(L)$) the solution is updated by the relaxation formula

$$ {}^{N}\phi_{K}^{+L} = \omega S(L) + (1-\omega)\, {}^{N}\phi_{K}^{L} \qquad (16) $$

where the values used for the last term are those from the previous iteration.

The next step is to use the periodicity conditions (upstream and downstream of the blades) and the blade-surface boundary conditions (within the blade row) in order to set the proper values at $L = 1$ and $L = LMX$. These are taken up, in turn, in the paragraphs below.

Periodicity Conditions

1. Upstream of the blade row:

   (a) here E(1) is set equal to zero, and F(1) is set equal to ${}^{N}\phi_{K}^{LMX}$

   (b) at $\zeta = 2\pi/B$: here the proper way to enforce periodicity is to re-write Equation (11), with ${}^{N}\phi_{K}^{LMX-1}$ replaced by ${}^{N}\phi_{K}^{2}$:

   $$ B_K^{LMX}\, {}^{N}\phi_{K}^{+LMX} + C_K^{LMX}\, {}^{N}\phi_{K}^{+LMX-1} = D_K^{LMX} - A_K^{LMX}\, {}^{N}\phi_{K}^{2} \qquad (17) $$

   The quantity ${}^{N}\phi_{K}^{+LMX-1}$ is then eliminated in favor of ${}^{N}\phi_{K}^{+LMX}$ by using Equation (13), resulting in an explicit relation for ${}^{N}\phi_{K}^{+LMX}$.

2. Downstream of the blade row:

In this region, it is necessary to account for the jump in potential and its radial derivative across the trailing vortex sheet (see Reference 8).

(a) here E(1) is set equal to zero, and F(1) is set equal to ${}^{N}\phi_{K}^{LMX} + \Delta\phi(N)$

(b) at $\zeta = 2\pi/B$: in order to evaluate the even part of the ζ -derivatives correctly, it is necessary to replace ${}^{N}\phi_{K}^{LMX+1}$ by ${}^{N}\phi_{K}^{2} - \Delta\phi$ (see Figure 4). The odd part also makes a contribution to $\phi_{\zeta\zeta}$ (see Equation (54), Reference 8); the net result is

$$\phi_{\zeta\zeta}^{LMX} = -\frac{\rho^2}{2(1+\rho^2)}\left\{\frac{\Delta\phi(N+1) - 2\Delta\phi(N) + \Delta\phi(N-1)}{(\Delta\rho)^2} + \frac{\Delta\phi(N+1) - \Delta\phi(N-1)}{2\rho\Delta\rho}\right\} + \frac{{}^{N}\phi_{K}^{2} + {}^{N}\phi_{K}^{LMX-1} - 2\,{}^{N}\phi_{K}^{LMX} - \Delta\phi(N)}{(\Delta\zeta)^2} \tag{18}$$

This formula is then used to derive an equation similar to Equation (17), from which an explicit relation for ${}^{N}\phi_{K}^{+LMX}$ can be found.

Blade-Surface Boundary Conditions

There are two options for specifying boundary conditions at the blade surfaces, designated by Roman numerals I and II:

I. Here the blade shape is specified. Thus, the surface slope (see Reference 8, Equation (43)) is given at all grid points on the suction and pressure sides of the blades.

(a) at $\zeta = 0$:

$$\left.\frac{d\eta}{ds}\right)_{L=1} = \left.\frac{u_n}{W_0}\right)_{L=1} = \frac{1}{\rho}\frac{\partial\phi}{\partial\zeta} - \frac{\rho}{1+\rho^2}\frac{\partial\phi}{\partial Z}$$

Thus,

$$\left.\frac{\partial\phi}{\partial\zeta}\right|_{\zeta=0} = \rho\left.\frac{d\eta}{ds}\right|_{\zeta=0} + \frac{\rho^2}{1+\rho^2}\left.\frac{\partial\phi}{\partial Z}\right|_{\zeta=0}$$

This is used to approximate $\phi_{\zeta\zeta}$, as follows:

$$\left.\phi_{\zeta\zeta}\right|_{\zeta=0} = \frac{2}{\Delta\zeta}\left[\frac{{}^{N}\phi_{K}^{+2} - {}^{N}\phi_{K}^{+1}}{\Delta\zeta} - \left.\phi_{\zeta}\right|_{\zeta=0}\right] \tag{19}$$

When this is substituted into the potential equation, at $\zeta = o$, and the result compared with Equation (13), an explicit relation for ${}^{N}\phi^{+}_{K}{}^{1}$ results.

(b) at $\zeta = 2\pi/B$: an analogous procedure is used here, the major difference being that the ζ -derivatives are replaced by:

$$\phi_{\zeta}\Big|_{\zeta = 2\pi/B} = \rho \frac{d\eta}{dS} + \frac{\rho^2}{1+\rho^2} \frac{\partial \phi}{\partial Z}\Big|_{\zeta = \zeta_1}$$

Thus,

$$\phi_{\zeta\zeta}\Big|_{\zeta = 2\pi/B} = \frac{2}{\Delta\zeta} \left(\phi_{\zeta}\Big|_{\zeta = 2\pi/B} - \frac{{}^{N}\phi^{+}_{K}{}^{LMX} - {}^{N}\phi^{+}_{K}{}^{LMX-1}}{\Delta\zeta} \right) \quad (20)$$

The analogous sequence of steps then leads to an expression for ${}^{N}\phi^{+}_{K}{}^{LMX}$.

II. Here the given quantities are values, at all grid points on the blade surfaces, of the loading ΔC_p and the thickness t , defined as: (see Reference 8, Equation (43))

$$\Delta C_p = \frac{p_L - p_u}{\frac{1}{2}\rho_\infty U_\infty^2} = -2\left(\frac{W_o}{U_\infty}\right)^2 \left\{ \frac{u_s}{W_o}\Big|_L - \frac{u_s}{W_o}\Big|_u \right\} \quad (21)$$

$$= -2(1+\rho^2) \frac{\phi_z|_{LMX} - \phi_z|_{L=1}}{1+\rho^2} = -2\phi_z|_{LMX} + 2\phi_z|_{L=1}$$

$$t'(s) = \frac{d\eta_u}{dS} - \frac{d\eta_L}{dS} = \frac{u_n}{W_o}\Big|_u - \frac{u_n}{W_o}\Big|_L \quad (22)$$

The first of these is used at $L = 1$, the second at LMX:

(a) at $\zeta = o$: Equation (21) can be rewritten as:

$${}^{N}\phi^{+}_{K}{}^{1} - {}^{N}\phi^{+}_{LE}{}^{1} = {}^{N}\phi^{+}_{K}{}^{LMX} - {}^{N}\phi^{+}_{LE}{}^{LMX} + \int_o^z \frac{\Delta C_p}{2} dz$$

But, from periodicity conditions, ${}^{N}\phi^{+}_{LE}{}^{1} = {}^{N}\phi^{+}_{LE}{}^{LMX}$, so the potential at $\zeta = o$ can be set from the formula:

$${}^{N}\phi^{+}_{K}{}^{1} = {}^{N}\phi^{+}_{K}{}^{LMX} + \int_o^z \frac{\Delta C_p}{2} dz \quad (23)$$

The integral appearing here is done once, at the start of the calculations.

(b) at $\zeta = 2\pi/B$: Equation (22) is rearranged, by expressing u_n in terms of ϕ_ζ and ϕ_z ; then ϕ_z is replaced in terms of ΔC_p . The result is

$$\phi_\zeta|_{LMX} = \phi_\zeta|_{L=1} - \frac{\rho^2}{1+\rho^2} \cdot \frac{\Delta C_p}{2} - \rho t'(s) \qquad (24)$$

This expression is then used to approximate $\phi_{\zeta\zeta}|_{LMX}$, as in Equation (20), and the result is substituted into the potential equation at LMX, leading to an explicit relation for ${}^N\phi_K^{+\,LMX}$.

Blade Loading

The force per unit span acting normal to the blade chord can be related to the jump in potential (see Figure 5).

$$\frac{dF_n}{dr} = \int_0^c (p_L - p_u)\, ds = 2\,\frac{1}{2}\,\rho_\infty u_\infty^2 \sqrt{1+\rho^2}\,\frac{u_\infty}{\omega}\,\Delta\phi(\rho) \qquad (25)$$

The quantity $\Delta\phi$ is also related to the circulation

$$\Gamma = \int_0^c (u_s|_u - u_s|_L)\, ds = \frac{u_\infty^2\,\Delta\phi(\rho)}{\omega} \qquad (26)$$

Blade Shape

When the calculations are done with prescribed thickness and loading distributions, the blade shape must be found after the solution converges. This is done by integrating the condition

$$\frac{d\eta_u}{ds} = \frac{u_n}{W_0} \quad ; \quad \frac{\eta_{u,L}}{C_a} = \frac{u_\infty}{\omega C_a}\sqrt{1+\rho^2}\int_0^z \frac{u_n}{W_0}\Big)_{u,L} dz \qquad (27)$$

The trapezoidal rule was used for these integrations.

Far-Field Conditions

The boundary condition used at $z \to -\infty$ is that the perturbation potential be zero. This is done by setting ${}^N\phi_1^L = 0$ for all N and L , where the station corresponding to $K = 1$ is taken several chord lengths upstream of the leading edge.

The condition that there be no disturbances upstream is correct for flows where $W_0/a_\infty < 1$. However, for the supersonic-tip case, where $W_0/a_\infty > 1$, the proper condition is a radiation condition, i.e., for $u_\infty/a_\infty < 1$, it is required that any waves present in the flow must have come from the blade row. At the present time, this condition has not been incorporated; thus, the solutions are restricted to cases where tip Mach number is subsonic.

At large distances downstream of the blade row, the perturbation quantities are required to be independent of z, at constant ζ, i.e., they do not change in the direction along the helical paths. This is enforced by selecting values of ϕ at $K = KMX$, equal to the constant value required for mass conservation (see Reference 8, Equation (56)).

$$ {}^{N}\phi^{+L}_{KMX} = \frac{C - DAF \cdot {}^{N}\phi^{+L}_{KMX-2} - DBF \cdot {}^{N}\phi^{+L}_{KMX-1}}{DCF} \tag{28} $$

where

$$ DAF = (z_{KMX} - z_{KMX-1}) / (z_{KMX-1} - z_{KMX-2})(z_{KMX} - z_{KMX-2}) $$

$$ DBF = (z_{KMX} - z_{KMX-2}) / (z_{KMX-1} - z_{KMX-2})(z_{KMX-1} - z_{KMX}) $$

$$ DCF = (2z_{KMX} - z_{KMX-1} - z_{KMX-2}) / (z_{KMX} - z_{KMX-2})(z_{KMX} - z_{KMX-1}) $$

Hub and Shroud Conditions

In general, the boundary conditions at the hub and shroud require that the radial derivative of the potential be proportional to the slope of the surface. For the present formulation, these surfaces are taken to be cylinders; thus, the requirement is that $\partial\phi/\partial\rho = 0$. This is enforced by setting ϕ at $N = 1$ and $N = NMX$ such that the derivative is zero, i.e.,

$$ {}^{1}\phi^{L}_{K} = \frac{4}{3}\,{}^{2}\phi^{L}_{K} - \frac{1}{3}\,{}^{3}\phi^{L}_{K} $$

$$ {}^{NMX}\phi^{L}_{K} = \frac{4}{3}\,{}^{NMX-1}\phi^{L}_{K} - \frac{1}{3}\,{}^{NMX-2}\phi^{L}_{K} \tag{29} $$

Updating of the Jump in Potential

When the calculations are being done in the mode where the geometry is given, the quantity $\Delta\phi(\rho)$ is updated as the calculation proceeds, in the manner outlined by Ballhaus and Bailey[16].

$$\Delta \overset{+}{\phi}(\rho) = \omega_p \left\{ \overset{+}{\phi}\left(\frac{\omega C_a}{U_\infty}, \rho, 0 \right) - \overset{+}{\phi}\left(\frac{\omega C_a}{U_\infty}, \rho, \frac{2\pi}{B} \right) \right\} + (1-\omega_p)\Delta\phi(\rho) \quad (30)$$

The relaxation factor ω_p used here is taken equal to $3/KMX$, since a monotone convergent sequence of iterations will behave according to

$$y_n \rightarrow y_{FINAL} \left[1 - e^{-\omega_p \cdot ITK} \right]$$

where ITK counts the iterations in the axial direction. Since the total number of sweeps in the axial directions is usually chosen to be of the order of KMX, the above choice of ω_p will assure that the argument of the exponential factor is sufficiently large.

Because the perturbation velocity components are forced to be periodic downstream of the trailing edge, the values of ϕ at the trailing edge that enter Eq. 30 will tend toward the value of $\Delta\phi$ required by the Kutta condition, i.e., the value that makes the perturbation pressures at $\zeta = 0$ and $\zeta = 2\pi/\beta$ equal. This condition can be enforced more strongly by selecting $\Delta\phi$, at each iteration, to be precisely the value that will make the perturbation pressures equal at the trailing edge. If subscripts a and b denote the locations of the last two points on the airfoil, this value is:

$$\Delta\phi^* = \frac{\left\{ -(Z_{TE} - Z_b)^2 \Delta\phi_a + (Z_{TE} - Z_a)^2 \Delta\phi_b \right\}}{(Z_b - Z_a)(2Z_{TE} - Z_a - Z_b)}$$

where $Z_{TE} = \omega C_a / U_\infty$

$$\Delta\phi_{a,b} = \overset{+}{\phi}(Z_{a,b}, \rho, 0) - \overset{+}{\phi}\left(Z_{a,b}, \rho, \frac{2\pi}{\beta} \right)$$

The computer program contains an option for using this formula. Under this option, ω_p is read in, and $\Delta\phi$ is updated by

$$\overset{+}{\Delta\phi} = \omega_p \Delta\phi^* + (1-\omega_p)\Delta\phi$$

A limited number of runs, made with this option, showed only minor differences from those which used Eq. 30. All of the results presented below used Eq. 30.

Grid Used

The grid used for the calculations reported here had a uniform spacing in the ρ- and ζ-directions. The grid was unevenly spaced in the z-direction, as follows: the upstream and downstream boundaries were set at

$$z_B = -2\,\frac{\omega C_a}{u_\infty} \quad , \quad z_I = +3\,\frac{\omega C_a}{u_\infty}$$

Then the intermediate points were located at

$$z(K) = z_M + \frac{1}{2\alpha}\,\ln\left[\frac{K\Delta\tau}{2 - K\Delta\tau}\right], \quad K = 1, 2, \ldots, KMX \qquad (31)$$

where

$$z_M = \frac{1}{2}\,(z_I + z_B)$$

$$\Delta\tau = 2/(KMX + 1)$$

$$2\alpha = \frac{\ln\left[\Delta\tau/(2 - \Delta\tau)\right]}{\left[-2\,\frac{\omega C_a}{u_\infty} - z_M\right]}$$

Relaxation Factors

In updating the points on a given line (z = constant, ρ = constant, $0 \le \zeta \le 2\pi/B$) the relaxation factor was taken as either of two values, depending on whether there were any hyperbolic points on that line. If there were, a hyperbolic relaxation factor was used; if all the points were elliptic, an elliptic relaxation factor was used.

The hyperbolic relaxation factor, called RXH , was read in as a constant, less than 1.0. The elliptic relaxation factor was taken as a function of $\bar{z}$, which varied from an input maximum value, called RXE , to the value 1.0 at large distances upstream and downstream of the blades, according to the formula:

$$\omega = 1.0 + (RXE - 1) \exp\left\{-\left(\frac{\bar{z} - \frac{1}{2}\,\frac{\omega C_a}{u_\infty}}{\omega C_a / u_\infty}\right)^2\right\} \tag{32}$$

When this was not done, it was found that values of the potential far upstream and far downstream did not converge.

II. RESULTS

The computer program described above has been used to carry out two calculations, for the purpose of demonstrating its capabilities.* The blade row used for both of these calculations is shown in Figure 6. It had 30 blades, with a hub-to-tip radius ratio of 0.5 and a solidity c_a/L_T of 0.5. Both calculations used an axial Mach number of 0.4, and an angular Mach number at the tip of 0.8, making the resultant Mach number at the tip 0.894. The grid used for these calculations had 40 points in the $\bar{z}$ -direction, 20 points in the ζ -direction, and 10 points radially, for a total of 8000 grid points. Constant grid spacings were used in the ρ - and ζ -directions; a variable grid was used in the $\bar{z}$ -direction, with points more closely spaced in the vicinity of the blades (14 of the 40 points lay between the leading- and trailing-edge stations). The grid extended from $2c_a$ upstream of the leading-edge station to $2c_a$ downstream of the trailing-edge station, as noted in Section I.

The relaxation procedure began by finding the solution at the hub. Line relaxation was used, with all points on the line $\bar{z}$ = constant, ρ = constant updated simultaneously. This line is then swept from upstream to downstream, and the sweep is repeated a number of times, typically the same as the number of grid points in the $\bar{z}$ -direction, in order for information to be carried from one end of the grid to the other. The solution then proceeds to the next radius, where the process is repeated. After this first sequence of radial iterations has reached the tip radius, it is then repeated. The number of repetitions is typically the same as the number of radial surfaces in the grid. This procedure is analogous to one which has been used for isolated-wing calculations.[17]

The program was written in FORTRAN IV and, using the H compiler, was run on the IBM 370/168 of the Martin-Marietta Corporation Great Lakes Data Center. It was found that the computing time required was 36 microseconds per

*An earlier version of these results, calculated with a non-conservative difference scheme, was presented in Ref. 16.

grid point per visitation, exclusive of the time required for output. Each of the two calculations reported below took about four minutes, plus the time used in output. (The latter time requires an additional 5 to 10 seconds, depending on the amount of output desired.)

First Case: Given Blade Shape

In the first demonstration calculation, the blade geometry was specified. The blades were taken to have parabolic-arc distributions of thickness and camber (see Figure 7).

$$\eta_{\mu}(s) = h(s) \pm \frac{1}{2} t(s)$$

$$t(s) = \frac{4\, t_{max}(r)}{[c(r)]^2} \left\{ s\,[c-s] \right\} \qquad (33)$$

$$h(s) = \frac{4\, h_{max}(r)}{[c(r)]^2} \left\{ s\,[c-s] \right\}$$

The maximum thickness was chosen as a constant, of such a magnitude that the variation of chord length with radius produces a thickness-to-chord ratio $t_{max}/c(r)$ which varies from 6% at the tip to 9.49% at the hub. The maximum camber was also chosen as a constant, of such a magnitude as to make the camber vary from 4% of the chord at the tip to 6.33% of the chord at the hub. The blade shapes at the hub and tip are shown in Figure 8.

The convergence of the solution is shown in Figure 9, which presents the variation of the streamwise perturbation velocity at mid-chord, on the suction side of the blade. The iteration number shown here counts the number of times the values at a given point have been updated. The calculation was done in ten successive stages: most of these used two radial sweeps, with 20 axial sweeps on each radial one; on several of the stages, only one radial sweep was used, with 40 axial sweeps.

The relaxation factor ω_e (see Equation (10) was taken as 1.0; the quantity RXH was chosen as 0.9, while RXE was set equal to 1.0 for the first 120 iterations, and equal to 1.2 thereafter. Several attempts were made, at later stages of the solution, to increase RXE to 1.4, but these led to divergent behavior.

The results of this calculation show that the flow accelerates to locally supersonic conditions over the outer half of the span. Contours of the local Mach number are shown in Figures 10a and 10b for radial stations near the hub and near the tip.

Second Case: Given Thickness and Loading

The second demonstration calculation was done using the computer program in the design mode. The thickness distribution was chosen to be the same as used in the above calculation, while the loading distribution had the form shown in Figure 11. The value of $\Delta C_{p_o}(r)$ varied linearly between prescribed values at the hub and tip.* The values used were $a = 0.6$, $\Delta C_{p_o} = 0.5$ at the hub, and 1.0 at the tip. The flow resulting from these specifications was everywhere subsonic; contours of the local Mach number at two radial stations are given in Figures 12a and 12b.

The convergence of the solution is shown in Figure 13, using the same location as in Figure 9. The relaxation factors ω_e and RXH were again chosen as 1.0 and 0.9. However, it was found that the relaxation factor used for elliptic points had to be quite small at the beginning of the calculation. The values used were:

Iteration Number	RXE
1-200	0.1
201-400	0.4
401-1000	0.8

The blade shape required to achieve this loading is shown in Figure 14 for the hub and tip. It is interesting to note that an angle of attack makes up the largest portion of the blade shape, with only a modest contribution from camber.

---

*Strictly speaking, this distribution is inconsistent with the condition $v = o$ at the hub and tip, since it is always true that

$$v(\bar{z}, \rho, o) - v(\bar{z}, \rho, \frac{2\pi}{\beta}) = \frac{d}{d\rho} \Delta\phi\rho$$

As a consequence, the radial velocities calculated for this case are inaccurate near the hub and tip.

III. CONCLUDING REMARKS

The principal significance of the results presented above is that the first step spoken of in the introduction has been carried out: it is now possible to make three-dimensional transonic flow calculations of periodic flows in a compressor blade row. Because a relaxation method is used, the computing times required are quite modest. Further steps are now possible, in the directions of application and extension.

Some of the applications that need to be made are to compare the predictions of this method with experiment. As noted earlier, it can be expected that the small-disturbance theory will have a certain range of validity; the extent of this range, and the principal factors which limit it remain to be determined by comparisons with experimental data. In addition, there are several questions that can be answered by further application: among these are the effect of blade shape and loading on the location of supersonic zones, the types of camber-line distributions required to achieve various pressure distributions, and the degree of validity of quasi-two-dimensional solution methods. All of these questions can now be answered, in the small-disturbance approximation, by conducting a series of calculations in which the appropriate parameters are varied. The experience gained to date suggests that these calculations can be done at quite reasonable cost.

In addition, the availability of a three-dimensional inviscid solution makes it possible to consider the three-dimensional boundary-layer flow that would result. By examining the pressure distributions on the hub, shroud, and blade surfaces, the general features of these boundary layers can be described, and quantitative estimates of viscous losses can be made.

Looking beyond these applications, there are many extensions that can be made. Some of the most important ones are the inclusion of further nonlinear terms in the potential equation, which may enable consideration of

highly cambered blades, large turning angles, and pressure ratios substantially larger than 1.0. These extensions might also allow incorporation of further geometrical complications, such as rounded leading edges, part-span shrouds, tapered blades, and variations in the annular cross-section.

One of the major limitations of the present results is its poor representation of shock transitions. This problem can be overcome by the addition of a shock-fitting technique.[18,19] Once that has been done, the necessary tools will be at hand for studies of shock-wave/boundary layer interaction in a transonic compressor rotor.

Even with the full nonlinear potential equation, there are still a number of limiting assumptions, especially in regard to the absence of gradients in the inlet flow. An alternate formulation, recently been developed by McCune and Hawthorne,[20,21] is free from this restriction. This formulation uses small perturbations of the axisymmetric mean flow; it may be that the numerical solution of the perturbation equations in this formulation would be a profitable avenue to follow.

On an even longer time scale, there are many other techniques that have proven to be of great value in relaxation calculations of external flows, and which hold comparable promise for internal flows. For example, the area of convergence-acceleration techniques[22-24] can now be considered for three-dimensional turbomachinery flows, and use of a velocity-component formulation,[25-27] capable of treating flows with radial inlet gradients, can be contemplated. As was the case with external-flow calculations, the experience gained in the small-disturbance approximation, in regard to such matters as coordinate systems, periodicity, and rotated differences, helps to show how further advances can be made.

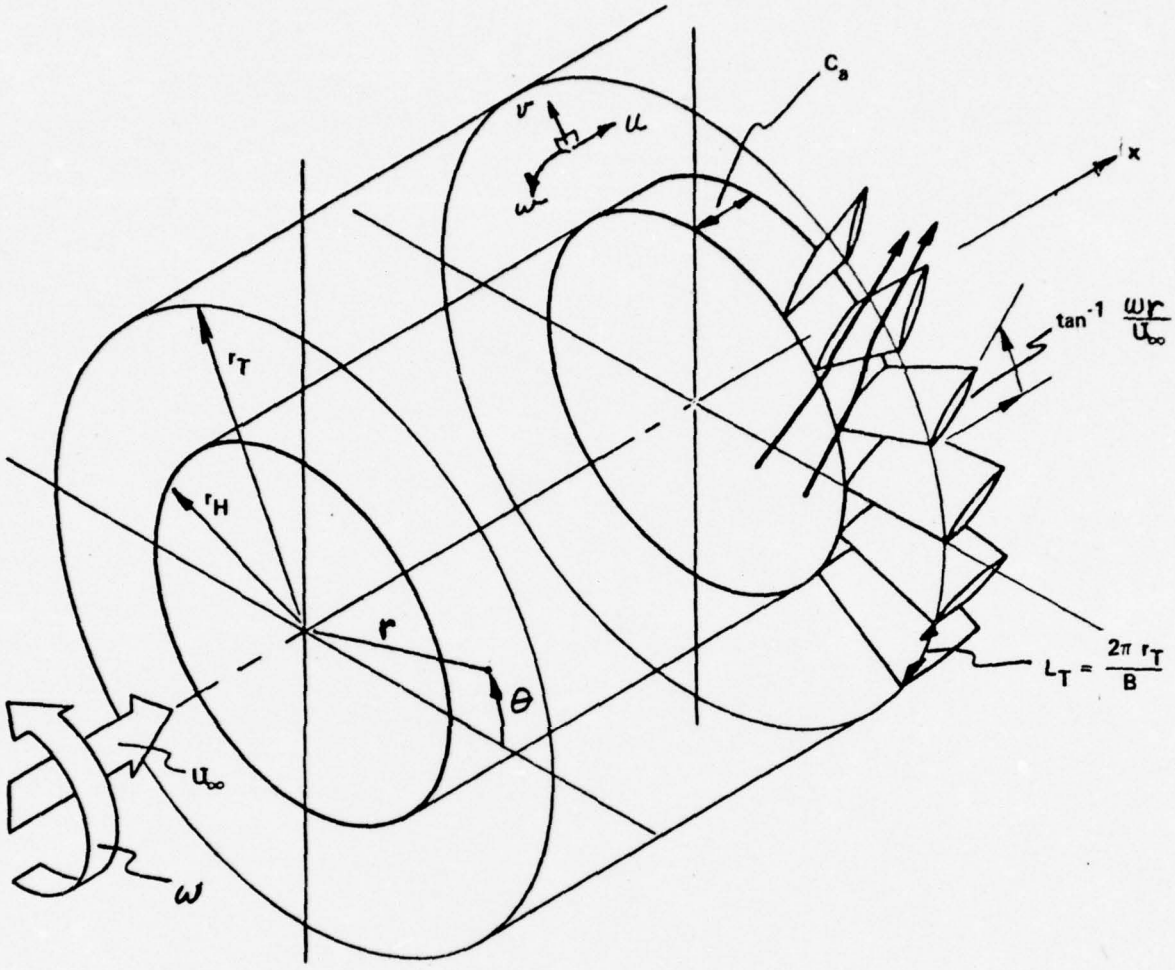

Figure 1 BLADE-FIXED COORDINATES

ROTOR IS STATIONARY IN A HELICAL APPROACH FLOW

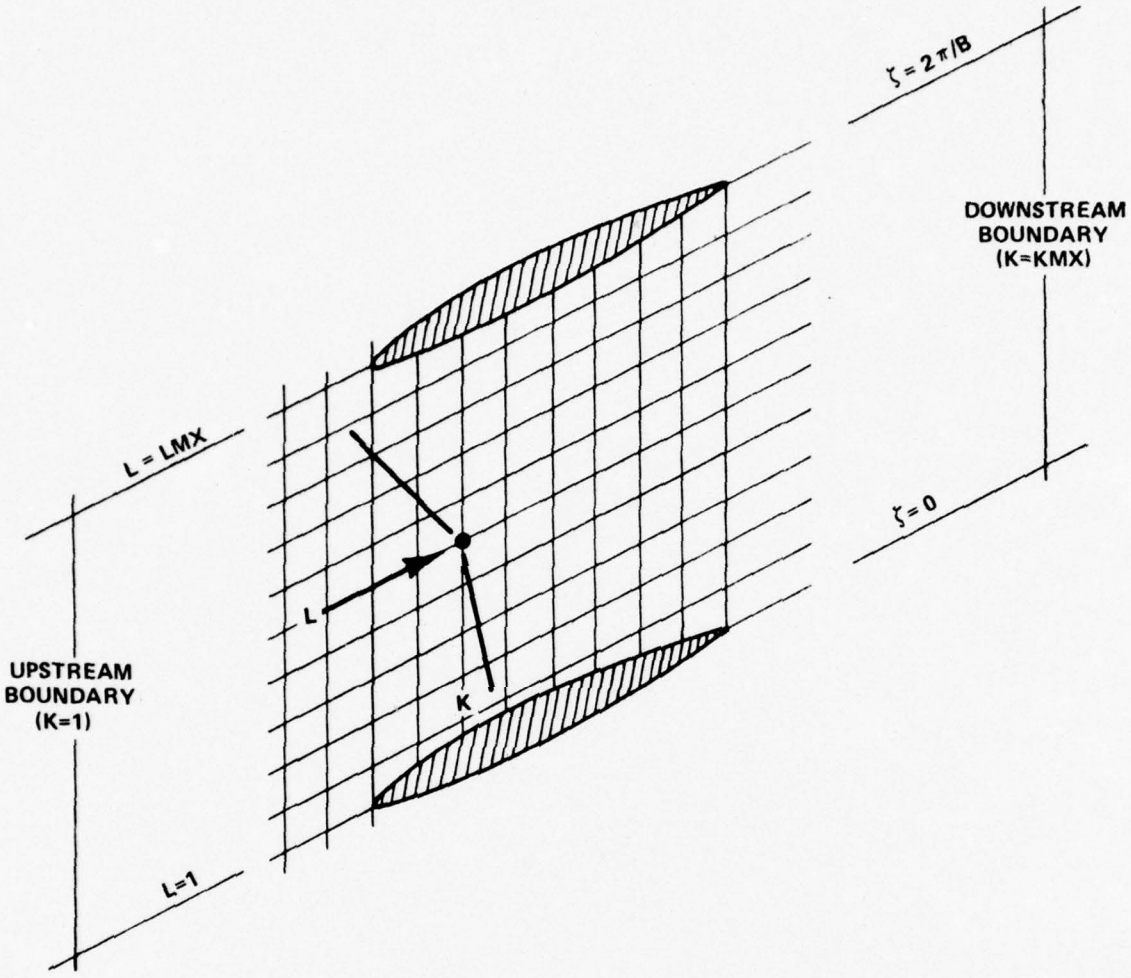

Figure 2 COORDINATE SYSTEM AND FINITE-DIFFERENCE GRID, SHOWING FORWARD MACH CONE AT POINT K, L. SURFACE SHOWN IS AT CONSTANT RADIUS (N = CONSTANT)

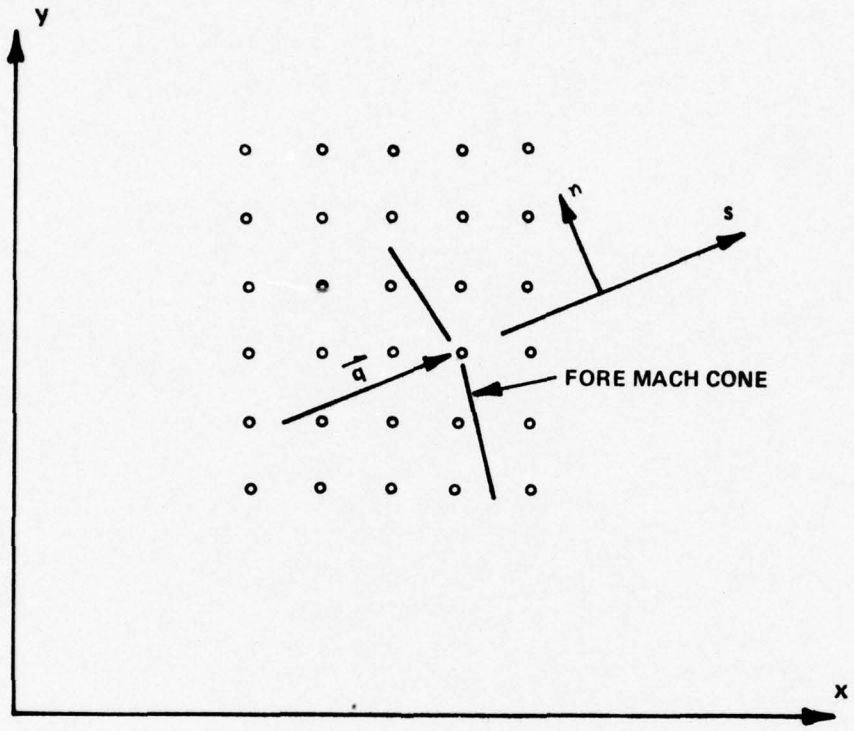

Figure 3 RECTANGULAR GRID, SHOWING MISALIGNMENT BETWEEN FLOW DIRECTION AND COORDINATE DIRECTIONS.

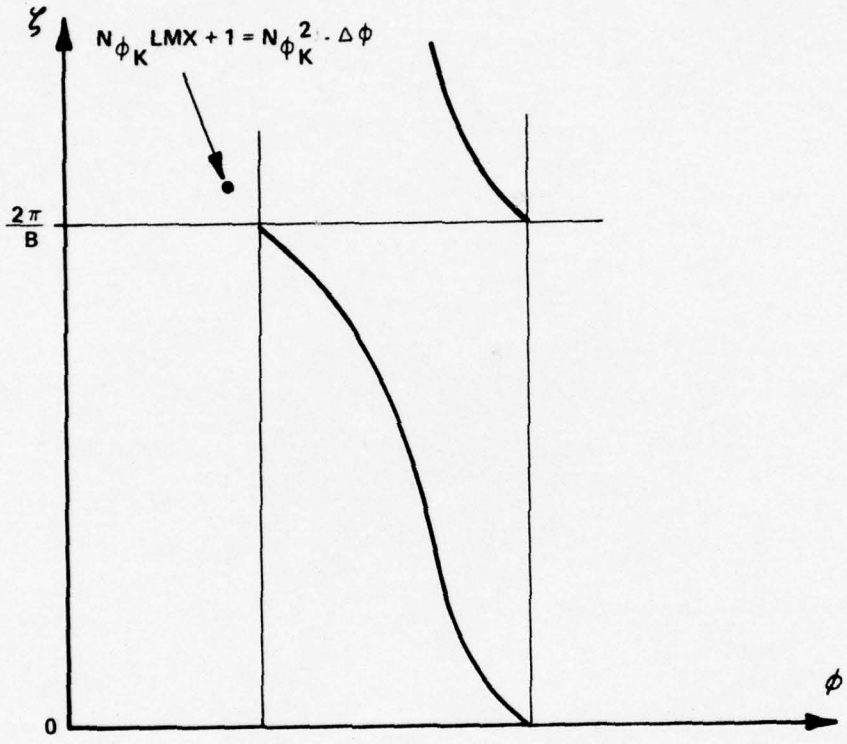

Figure 4 JUMP IN POTENTIAL ACROSS THE TRAILING VORTEX SHEET

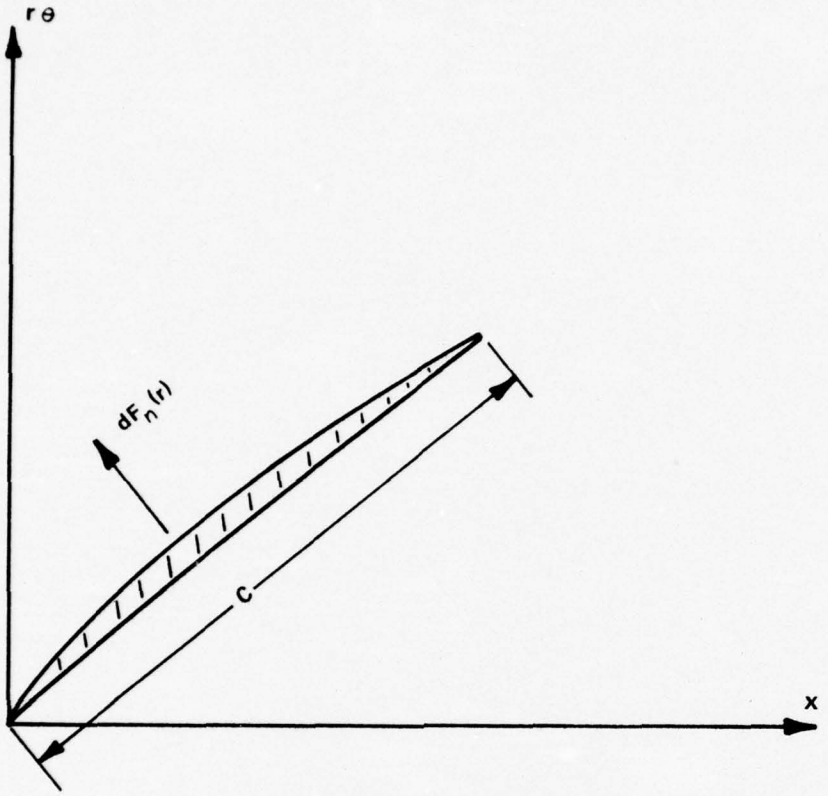

Figure 5 LOCAL NORMAL-FORCE DIRECTION

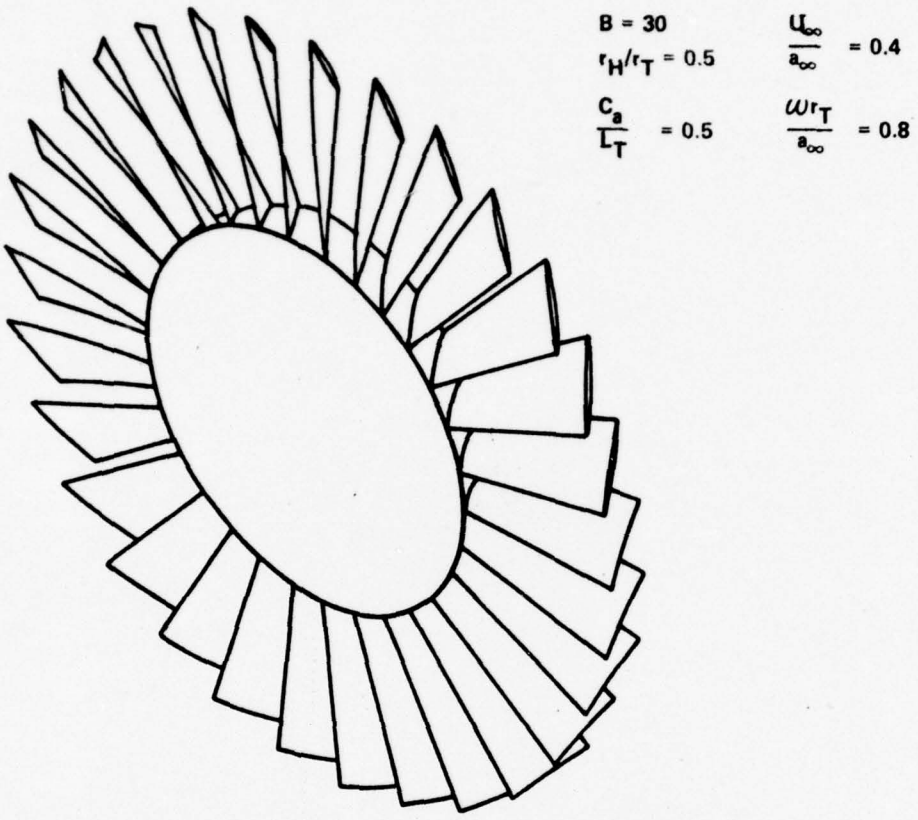

Figure 6 BLADE ROW USED FOR DEMONSTRATION CALCULATIONS

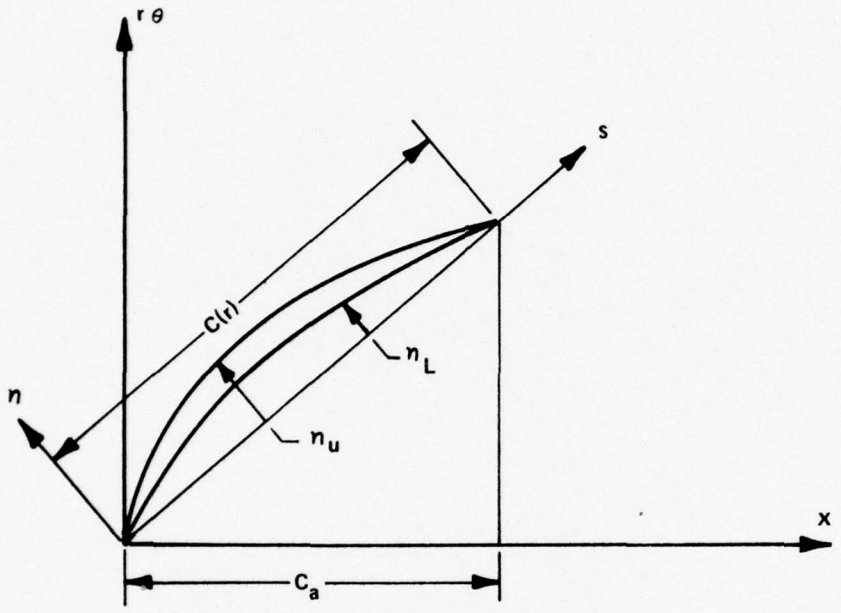

Figure 7 DEFINITIONS OF BLADE-SURFACE GEOMETRY

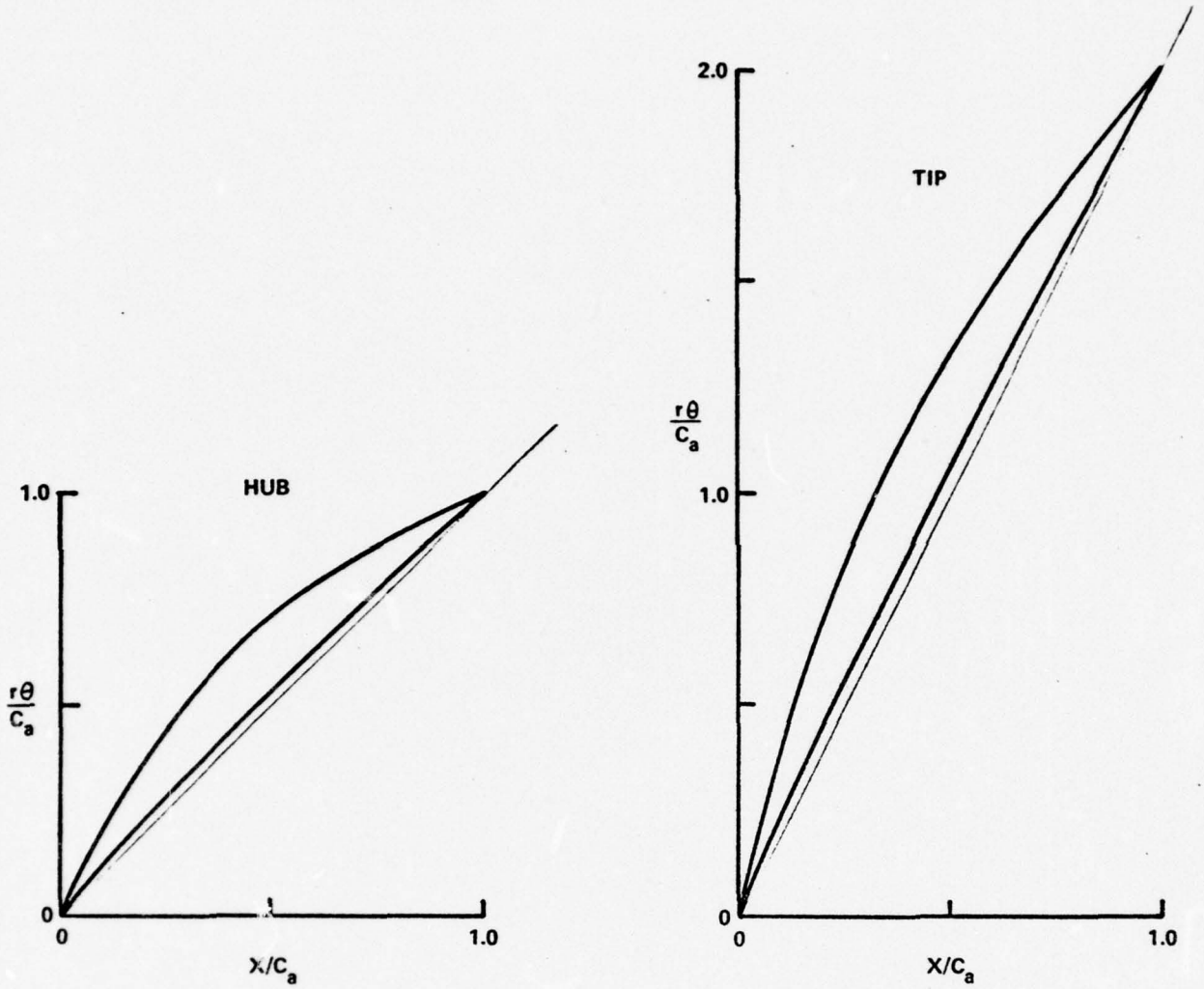

Figure 8 BLADE GEOMETRY SPECIFIED FOR 1ST DEMONSTRATION CALCULATION

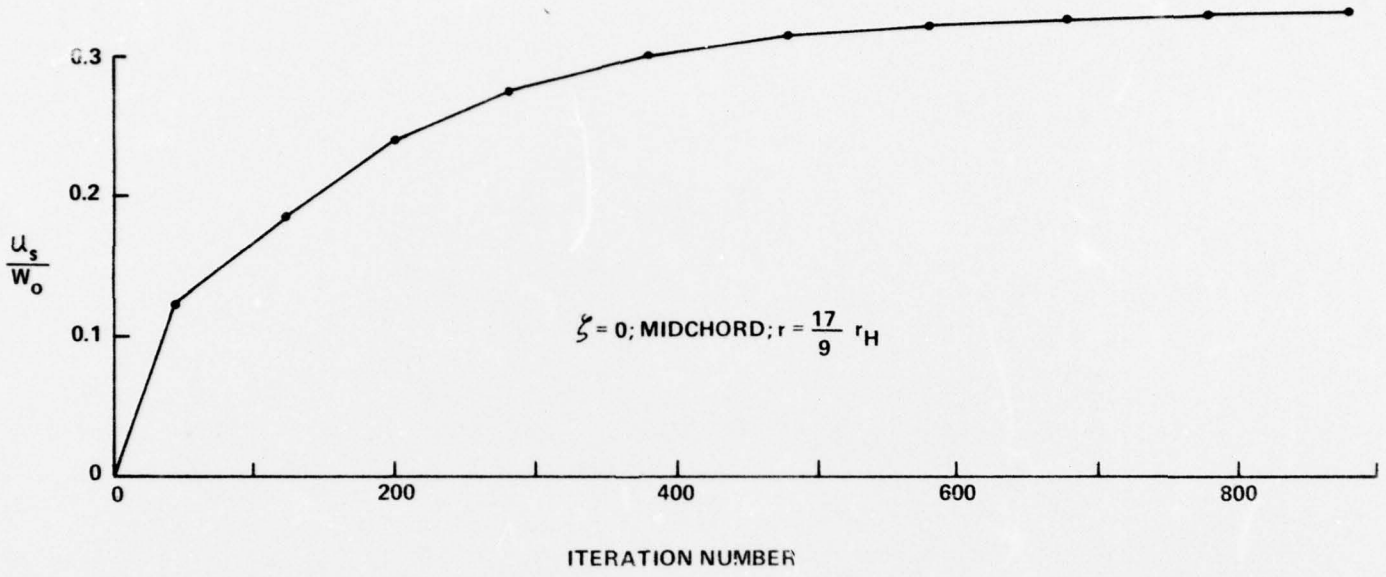

Figure 9 CONVERGENCE RATE FOR FIRST DEMONSTRATION CASE

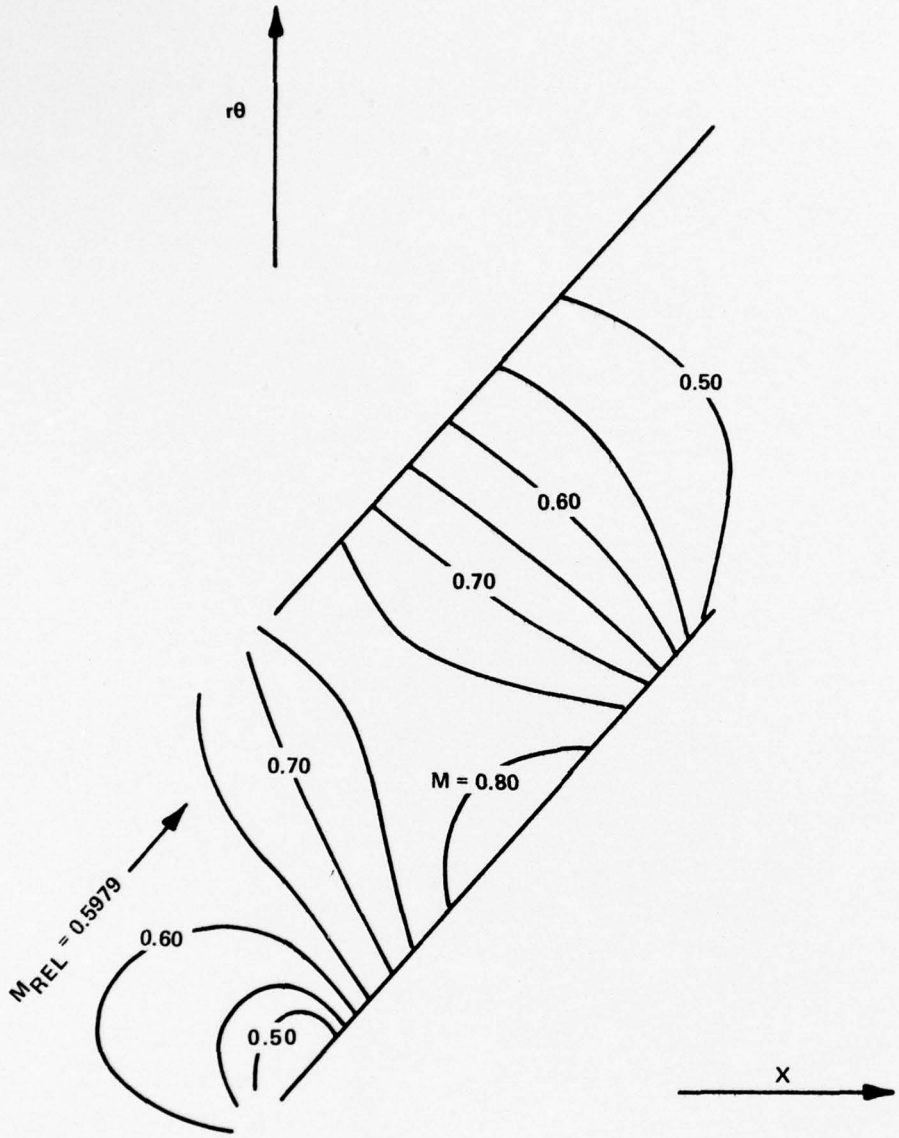

Figure 10a CONTOURS OF THE LOCAL MACH NUMBER
1ST DEMONSTRATION CALCULATION

$r = \frac{10}{9} r_{HUB}$

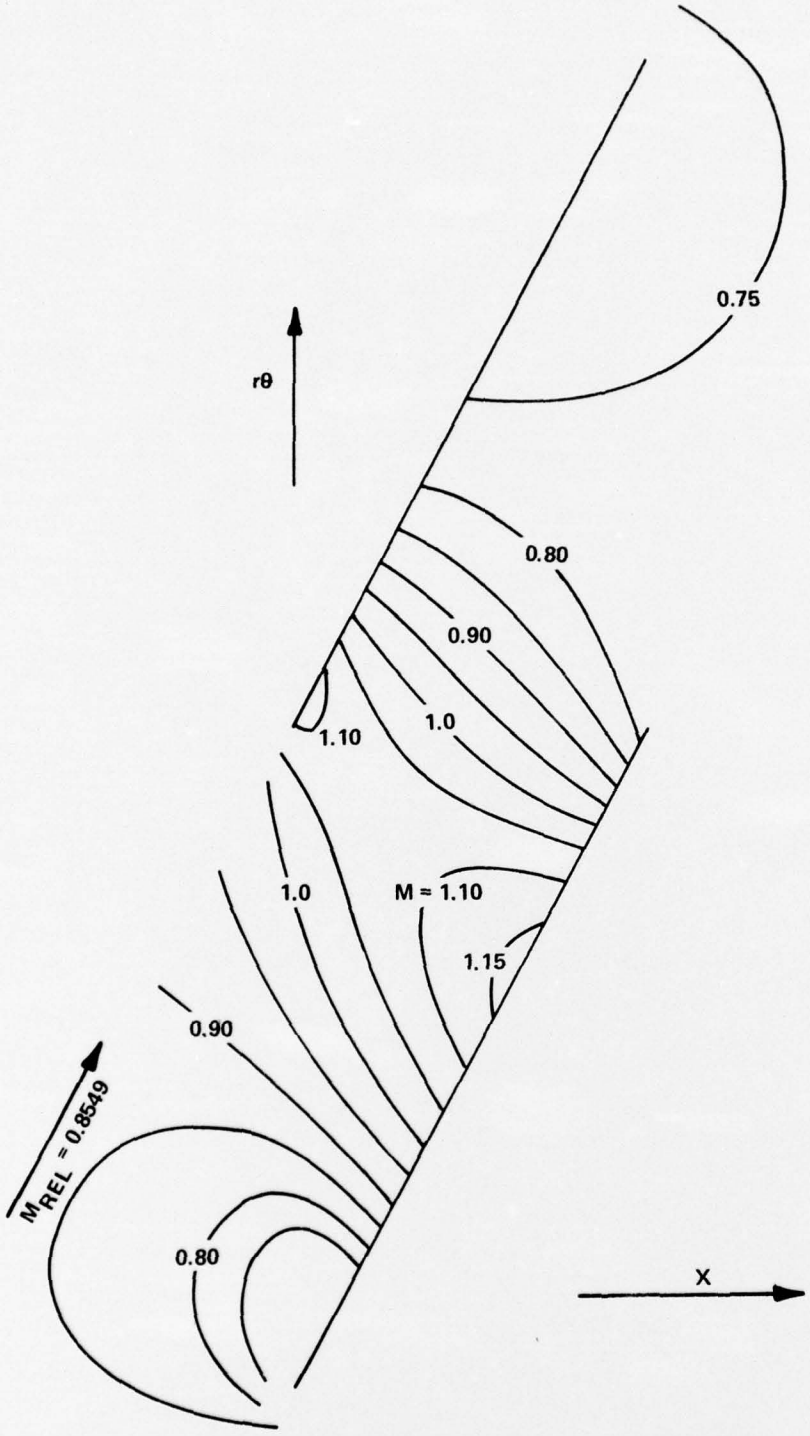

Figure 10b CONTOURS OF THE LOCAL MACH NUMBER
1ST DEMONSTRATION CALCULATION
$r = \frac{17}{9}\ r_{HUB}$

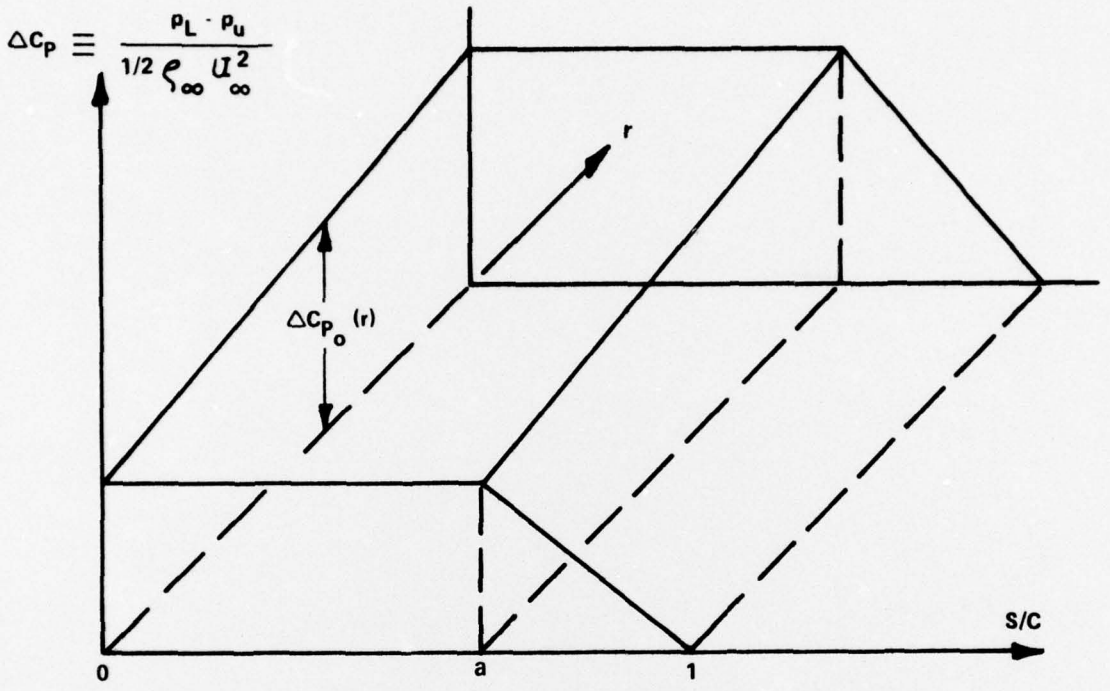

Figure 11 LOADING DISTRIBUTION USED FOR SECOND DEMONSTRATION CALCULATION

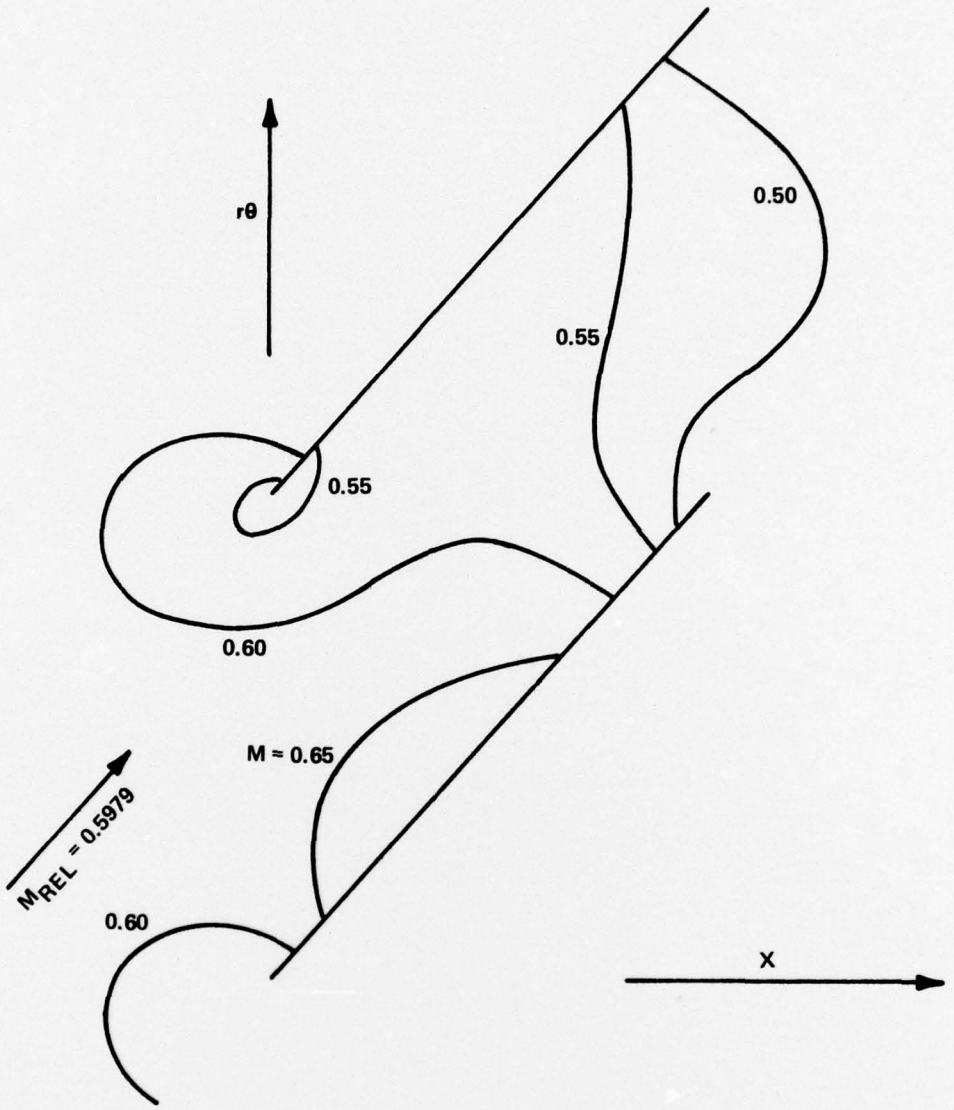

Figure 12a CONTOURS OF THE LOCAL MACH NUMBER
2ND DEMONSTRATION CALCULATION

$$r = \frac{10}{9} r_{HUB}$$

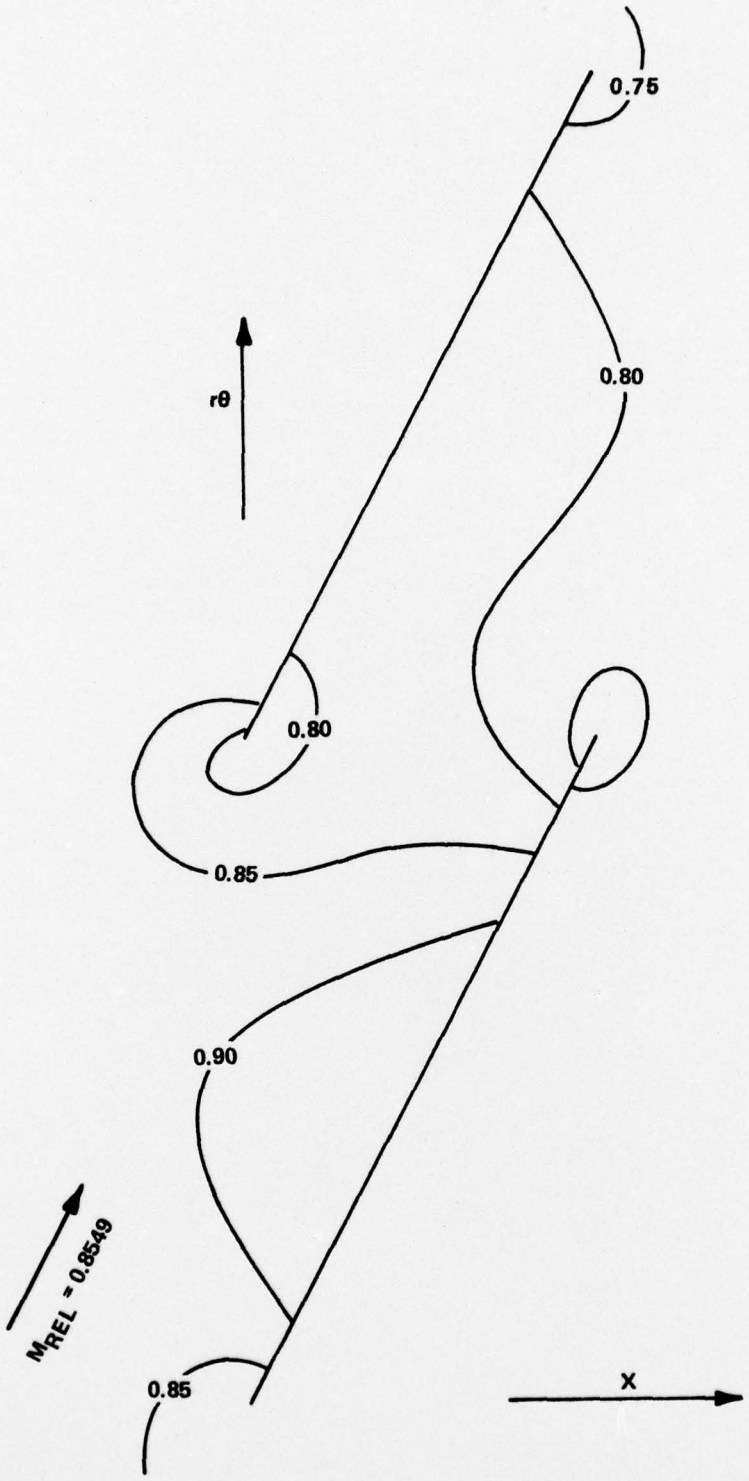

Figure 12b CONTOURS OF THE LOCAL MACH NUMBER
2ND DEMONSTRATION CALCULATION
$r = \frac{17}{9} r_{HUB}$

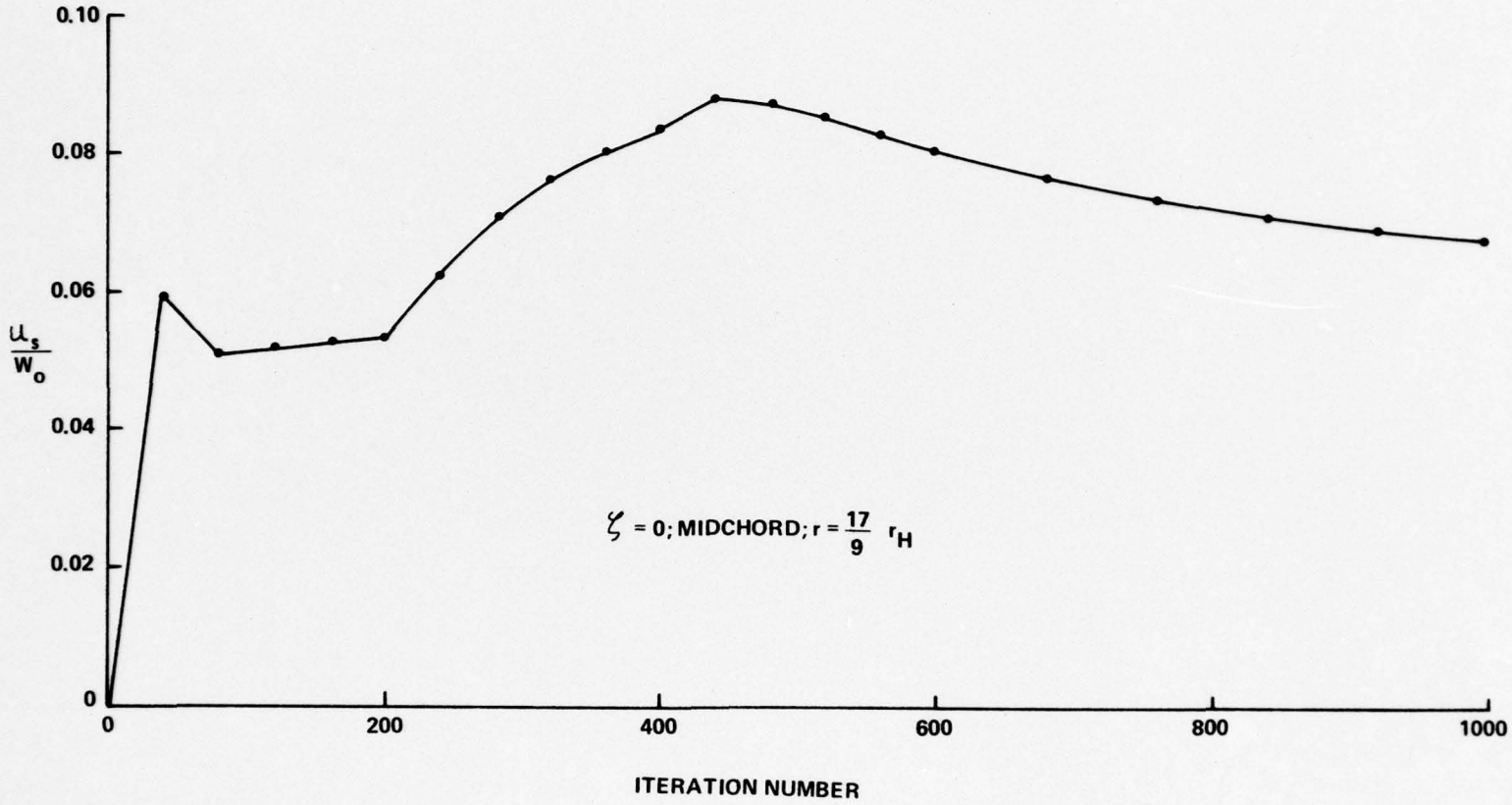

Figure 13 CONVERGENCE RATE FOR SECOND DEMONSTRATION CASE

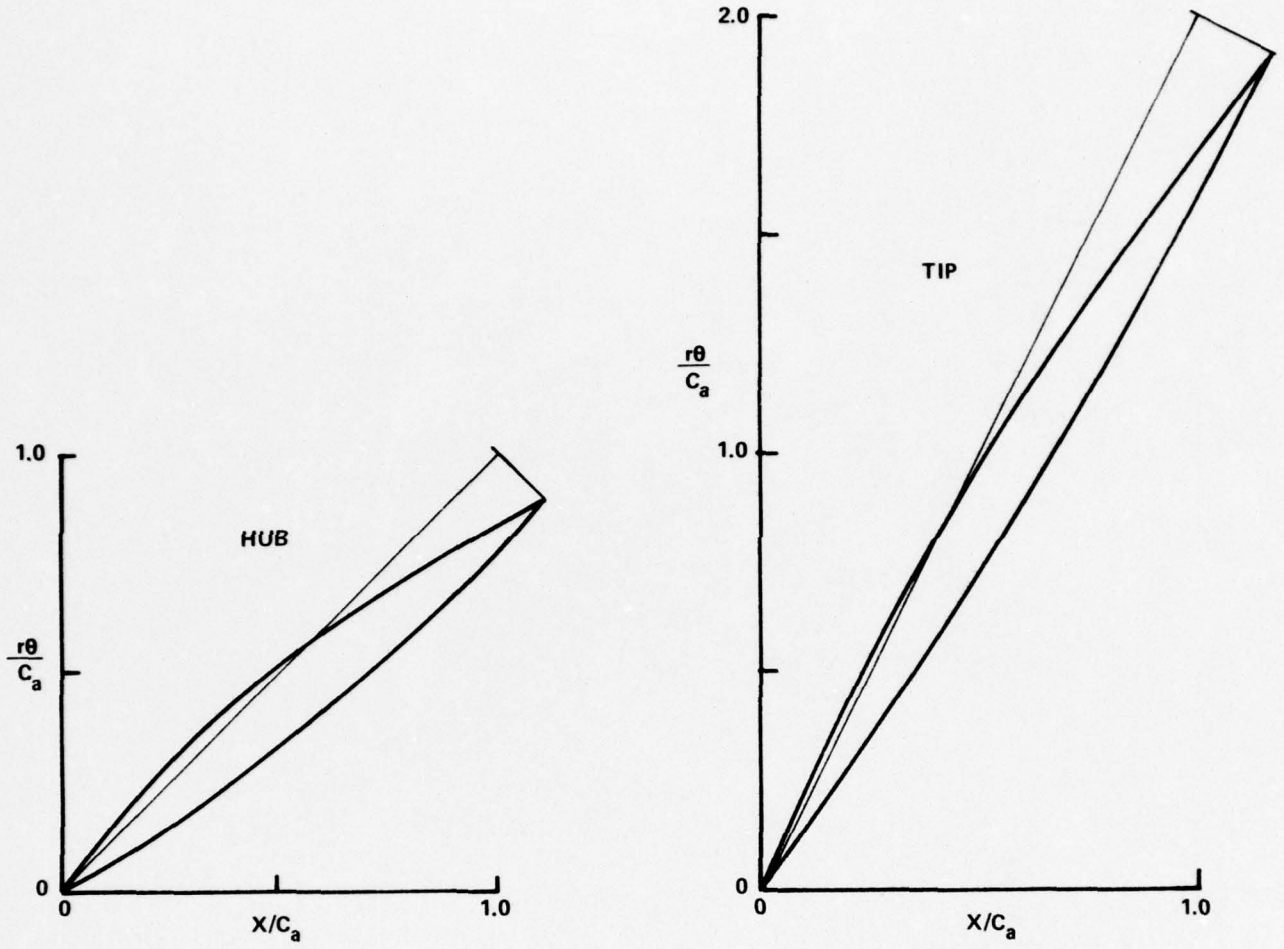

Figure 14 BLADE GEOMETRY FOUND FROM 2ND DEMONSTRATION CALCULATION

REFERENCES

1. Johnsen, I.A. and Bullock, R.O., eds. Aerodynamic Design of Axial-Flow Compressors, NASA SP-36, 1965.

2. Hartmann, M.J., Benser, W.A., Hauser, C.H. and Ruggeri, R.S., "Fan and Compressor Technology", pp. 1-36 of Aircraft Propulsion, proceedings of a conference held at NASA/Lewis Research Center, November 18-19, 1970, NASA SP-259, 1971.

3. Povinelli, F.P., Klineberg, J.M. and Kramer, J.J., "Improving Aircraft Energy Efficiency", Aeronautics and Astronautics 14, No. 2 (February 1976), 18-31.

4. Krupp, J.A., "The Numerical Calculation of Plane Steady Transonic Flows Past Thin Lifting Airfoils", Boeing Scientific Research Laboratories, Report D180-12958-1, June 1971.

5. Murman, E.M., and Cole, J.D., "Calculation of Plane Steady Transonic Flows", AIAA Journal 9, 1971, pp. 114-121.

6. Murman, E.M. and Krupp, J.A., "Solution of the Transonic Potential Equation Using a Mixed Finite Difference System", Proceedings of the Second International Conference on Numerical Methods in Fluid Dynamics, published as Vol. 8 of Lecture Notes in Physics, Springer-Verlag, 1971, pp. 199-206.

7. Krupp, J.A. and Murman, E.M., "Computation of Transonic Flows Past Lifting Airfoils and Slender Bodies", AIAA Journal 10, 1972, pp. 880-886.

8. Rae, W.J., "Nonlinear Small-Disturbance Equations for Three-Dimensional Transonic Flow Through a Compressor Blade Row", to Calspan Report No. AB-5487-A-1 (Aug. 1976).

9. Jameson, A., "Iterative Solution of Transonic Flows over Airfoils and Wings, Including Flows at Mach 1", Communications on Pure and Applied Mathematics 27, (1974), pp. 283-309.

10. Jameson, A., "Numerical Calculation of the Three-Dimensional Transonic Flow over a Yawed Wing", Proceedings of the AIAA Computational Fluid Dynamics Conference, (July 1973), pp. 18-26.

11. South, J.C. and Jameson, A., "Relaxation Solutions for Inviscid Axisymmetric Transonic Flow over Blunt or Pointed Bodies", Proceedings of the AIAA Computational Fluid Dynamics Conference, (July 1973), pp. 8-17.

12. Murman, E.M., "Analysis of Embedded Shock Waves Calculated by Relaxation Methods", Proceedings of the AIAA Computational Fluid Dynamics Conference (July 1973), pp. 27-40.

13. Newman, P.A. and South, J.C., "Conservative versus Nonconservative Differencing: Transonic Streamline Shape Effects", NASA TMX-72827 (February 1976).

14. Jameson, A., "Transonic Potential Flow Calculations Using Conservation Form", Proceedings of the AIAA 2nd Computational Fluid Dynamics Conference, (June 1975).

15. Richtmeyer, R.D. and Morton, K.W., Difference Methods for Initial-Value Problems, 2nd Ed., Interscience Publishers, New York (1967), pp. 198-201.

16. Rae, W.J. "Finite-Difference Calculations of Three-Dimensional Transonic Flow through a Compressor Blade Row, Using the Small-Disturbance Nonlinear Potential Equation" Paper presented at the Workshop on Transonic Flow Problems in Turbomachinery, U.S. Naval Postgraduate School, Monterey, California, Feb. 11-12, 1976.

17. Ballhaus, W.F. and Bailey, F.R. "Numerical Calculation of Transonic Flow about Swept Wings" AIAA Paper 72-677, June 1972.

18. Hafez, M.M. and Cheng, H.K., "Convergence Acceleration and Shock Fitting for Transonic Aerodynamics Computations", AIAA Paper 75-51 (January 1975), Corrigenda in Univ. of Southern California, School of Engineering Report USCAE 132 (April 1975).

19. Yu, N.J. and Seebass, A.R., "Computational Procedures for Mixed Equations with Shock Waves", Proceedings of the First International Conference on Computational Methods in Nonlinear Mecahnics (1974), pp. 499-508.

20. McCune, J.E., "Three-Dimensional Inviscid Flow Through a Highly-Loaded Transonic Compressor Rotor", Proceedings of a Workshop on Transonic Flow Problems in Turbomachinery, U.S.Naval Postgraduate School, February 1976, to be published.

21. McCune, J.E., and Hawthorne, W.R., "The Effects of Trailing Vorticity on the Flow Through Highly Loaded Cascades", J. Fluid Mech., in press (1976).

22. Steger, J.L. and Lomax, H., "Generalized Relaxation Methods Applied to Problems in Transonic Flows", Proceedings of the Second International Conference on Numerical Methods in Fluid Dynamics, published as Vol. 8 of Lecture Notes in Physics, Springer-Verlag, 1971, pp. 193-197.

23. Bailey, R.F. and Steger, J.L., "Relaxation Techniques for Three-Dimensional Transonic Flow about Wings", AIAA Paper 72-189, January 1972.

24. Steger, J.L. and Klineberg, J.M., "A Finite-Difference Method for Transonic Airfoil Design", AIAA Paper 72-679, June 1972.

25. Lomax, H. and Martin, E.D., "Fast Direct Numerical Solution of the Nonhomogeneous Cauchy-Riemann Equations", Journal of Computational Physics, 15, (1974), pp. 55-80.

26. Martin, E.D., "A Generalized-Capacity-Matrix Technique for Computing Aerodynamic Flows", Computers and Fluids 2 (1974), pp. 79-97.

27. Martin, E.D. and Lomax, H., "Rapid Finite-Difference Computation of Subsonic and Transonic Aerodynamic Flows", AIAA Paper 74-11 (1974).

DISTRIBUTION LIST FOR CALSPAN REPORT NO. AB-5487-A-2

Prof. Douglas E. Abbott
Purdue University
Thermal Sciences & Propulsion Center
West Lafayette, IN 47907

Dr. John Adamczyk
NASA Lewis Research Center
Cleveland, OH 44135

Dr. Thomas C. Adamson
College of Engineering
University of Michigan
Ann Arbor, MI 48105

Dr. Robert A. Arnoldi
United Technologies Corporation
Pratt & Whitney Aircraft Division
400 Main Street
East Hartford, CT 06108

Dr. Hafiz Atassi
University of Notre Dame
Department of Aerospace &
Mechanical Engineering
Notre Dame, IN 46556

Dr. F. R. Bailey
NASA Ames Research Center
Moffett Field, CA 94035

Dr. William Ballhaus
NASA Ames Research Center
Moffett Field, CA 94035

Prof. J. Chauvin
von Karman Institute
Rhode-Saint-Genese
Belgium

Prof. H. K. Cheng
School of Engineering
University of Southern California
Los Angeles, CA 90007

Dr. Julian Cole
University of California at Los Angeles
Los Angeles, CA 90024

Mr. Paul R. Dodge
AiResearch Manufacturing Company
Division of Garrett Corporation
402 So. 36th Street
Phoenix, AZ 85034

Dr. John Erdos
General Applied Science Laboratories
Westbury, NY 11590

Dr. J. C. Evvard
RFD 5, Box 127
Laconia, NH 03246

Mr. J. Fabri
ONERA
Chatillons-sous-Bagneux
92320 Chatillon
France

Dr. S. Fleeter
Detroit Diesel Allison
Indianapolis, IN 46206

Dr. Anthony A. Ganz
Pratt & Whitney Aircraft
400 Main Street
East Hartford, CT 06108

Dr. Wayland C. Griffith
North Carolina State University
School of Engineering
Raleigh, NC 27607

Dr. J. Gordon Hall
Department of Mechanical Engineering
State University of New York
at Buffalo
Buffalo, NY 14214

Dr. Wesley L. Harris
Massachusetts Institute of Technology
Cambridge, MA 02139

Prof. A. Hamed
University of Cincinnati
Cincinnati, OH 45221

Dr. G. David Huffman
Indianapolis Center for
Advanced Research
1300 West Michigan Street
Indianapolis, IN 46202

Dr. George R. Inger
Virginia Polytechnic Institute
and State University
Department of Aerospace and
Ocean Engineering
Blacksburg, VA 24061

Dr. David S. Ives
Pratt & Whitney Aircraft
400 Main Street
East Hartford, CT 06108

Dr. Antony Jameson
Courant Institute
New York University
New York, NY 10012

Dr. T. Katsanis
NASA Lewis Research Center
Cleveland, OH 44135

Dr. J. L. Kerrebrock
Gas Turbine Laboratory
Massachusetts Institute of Technology
Cambridge, MA 02139

Dr. John M. Klineberg
NASA Headquarters
600 Independence Avenue
Washington, DC 20546

Dr. James Krupp
Middlebury College
Middlebury, VT 05753

Dr. Metsuru Kurosaka
General Electric Company
R&D Center
Post Office Box 43
Schenectady, NY 12301

Prof. B. Lakshminarayana
Pennsylvania State University
State College, PA 16802

Prof. Frank E. Marble
California Institute of Technology
Division of Engineering &
Applied Sciences
Pasadena, CA 91109

Dr. William J. McCroskey
U. S. Army Air Mobility R&D Laboratory
Moffett Field, CA 94035

Mr. William D. McNally
NASA Lewis Research Center
Cleveland, OH 44135

Prof. James E. McCune
Massachusetts Institute of Technology
Department of Aeronautics &
Astronautics
Gas Turbine Laboratory
Cambridge, MA 02139

Dr. Robert Melnik
Grumman Aerospace Corporation
Bethpage, Long Island, NY 11714

Dr. Gino Moretti
Polytechnic Institute of New York
Farmingdale, NY 11735

Dr. Earll M. Murman
Flow Research, Inc.
1819 S. Central Avenue
Kent, WA 98031

Dr. S. N. B. Murthy
Project Squid Headquarters
Purdue University
West Lafayette, IN 47907

Dr. R. A. Novak
Northern Research and Engineering Corp.
219 Vassar Street
Cambridge, MA 02139

Dr. Gordon C. Oates
University of Washington
Seattle, WA 98105

Prof. T. H. Okiishi
Iowa State University of Science
and Technology
Department of Mechanical Engineering
Ames, IA 50010

Prof. R. E. Peacock
The School of Mechanical Engineering
Cranfield Institute of Technology
Cranfield, Bedford
England

Dr. M. F. Platzer
U. S. Naval Postgraduate School
Monterey, CA 93940

Prof. W. D. Rannie
Karman Laboratory
California Institute of Technology
Pasadena, CA 91109

Prof. B. M. Rao
Texas A&M University
Department of Aerospace Engineering
College Station, TX 77843

Prof. N. Rott
ETH
Zurich, Switzerland

Dr. A. R. Seebass
University of Arizona
Tucson, AZ 85721

Dr. Peter Sokol
NASA Lewis Research Center
Cleveland, OH 44135

Dr. J. C. South
NASA Langley Research Center
Hampton, VA 23665

Dr. Stephen S. Stahara
Nielsen Engineering & Research, Inc.
510 Clyde Avenue
Mountain View, CA 94040

Mr. H. Starken
Institut fur Luftstrahlantriebe
DFVLR
Porz-Wahn
West Germany

Mr. Marvin A. Stibich, AFAPL/TBC
Air Force Aero Propulsion Laboratory
Wright-Patterson Air Force Base
OH 45433

Prof. Demetri P. Telionis
Virginia Polytechnic Institute &
State University
Department of Engineering Sciences
& Mechanics
Blacksburg, VA 24061

Dr. W. E. Thompson
Turbo Research, Inc.
212 Welsh Pool Road
Lionville, PA 19353

Dr. Joseph M. Verdon
United Technologies Research Center
East Hartford, CT 06108

Mr. Leonard Walitt
Numerical Continuum Mechanics, Inc.
Suite 200
6269 Variel Avenue
Woodland Hills, CA 91364

Dr. A. Wennerstrom
Air Force Aero Propulsion Laboratory
Wright-Patterson Air Force Base
OH 45433

Dr. H. Yoshihara
Convair Division
General Dynamics Corporation
P.O. Box 80874
San Diego, CA 92138

Dr. N. J. Yu
University of Arizona
Tucson, AZ 85721

UNCLASSIFIED
SECURITY CLASSIFICATION OF THIS PAGE (When Data Entered)

REPORT DOCUMENTATION PAGE	READ INSTRUCTIONS BEFORE COMPLETING FORM
1. REPORT NUMBER: AFOSR - TR - 76 - 1081	2. GOVT ACCESSION NO. / 3. RECIPIENT'S CATALOG NUMBER
4. TITLE (and Subtitle): RELAXATION SOLUTIONS FOR THREE-DIMENSIONAL TRANSONIC FLOW THROUGH A COMPRESSOR BLADE ROW, IN THE NONLINEAR SMALL-DISTURBANCE APPROXIMATION	5. TYPE OF REPORT & PERIOD COVERED: INTERIM 6. PERFORMING ORG. REPORT NUMBER: AB-5487-A-2
7. AUTHOR(s): WILLIAM J RAE	8. CONTRACT OR GRANT NUMBER(s): F44620-74-C-0059
9. PERFORMING ORGANIZATION NAME AND ADDRESS: CALSPAN CORPORATION P O BOX 235 BUFFALO, NEW YORK 14221	10. PROGRAM ELEMENT, PROJECT, TASK AREA & WORK UNIT NUMBERS: 681307 9781-01 61102F
11. CONTROLLING OFFICE NAME AND ADDRESS: AIR FORCE OFFICE OF SCIENTIFIC RESEARCH/NA BUILDING 410 BOLLING AIR FORCE BASE, D C 20332	12. REPORT DATE: Aug 76 13. NUMBER OF PAGES: 43
14. MONITORING AGENCY NAME & ADDRESS (if different from Controlling Office)	15. SECURITY CLASS. (of this report): UNCLASSIFIED 15a. DECLASSIFICATION/DOWNGRADING SCHEDULE

16. DISTRIBUTION STATEMENT (of this Report)

Approved for public release; distribution unlimited.

17. DISTRIBUTION STATEMENT (of the abstract entered in Block 20, if different from Report)

18. SUPPLEMENTARY NOTES

19. KEY WORDS (Continue on reverse side if necessary and identify by block number)

TURBOMACHINERY
COMPRESSORS
TRANSONIC FLOW
FINITE-DIFFERENCE SOLUTIONS

20. ABSTRACT (Continue on reverse side if necessary and identify by block number)

A relaxation method for calculating the three-dimensional transonic flow through a compressor blade row is discribed. The flow is taken to be steady in blade-fixed coordinates, and is treated in the nonlinear small-disturbance approximation. Details of the finite-difference formulation and the solution procedure are given. The resulting computer code is capable of operating in either of two modes: in the first, the user specifies the complete blade shape and the operating conditions, and the program finds the complete flow field, including the loading distribution on the blades. In the second, the user specifies the loading distribution over

DD FORM 1 JAN 73 1473 EDITION OF 1 NOV 65 IS OBSOLETE

UNCLASSIFIED
SECURITY CLASSIFICATION OF THIS PAGE (When Data Entered)

the blade surface, and the thickness distribution of the blades. The program then finds the three-dimensional flow field, including the shape of the camber surface about which the prescribed thickness must be symmetrically distributed, in order to produce the prescribed loading. Results of demonstration calculations illustrating each of these modes are included.